BEYOND SEMICLASSICAL GRAVITY: QUANTUM STRESS TENSOR FLUCTUATIONS IN THE VACUUM

A dissertation submitted by

ENRICO D. SCHIAPPACASSE

in partial fulfillment of the requirements for the degree of

Doctor of Philosophy
in
Physics

Tufts University

May 2018

Adviser: Dr. Lawrence Ford

Abstract

Large vacuum fluctuations of a quantum stress tensor can be described by the asymptotic behavior of its probability distribution. Here we focus on stress tensor operators which have been averaged with a sampling function in time. The Minkowski vacuum state is not an eigenstate of the time-averaged operator, but can be expanded in terms of its eigenstates. We calculate the probability distribution and the cumulative probability distribution for obtaining a given value in a measurement of the time-averaged operator taken in the vacuum state. In these calculations, we use the normal ordered square of the time derivative of a massless scalar field in Minkowski spacetime as an example of a stress tensor operator. We analyze the rate of decrease of the tail of the probability distribution for different temporal sampling functions, such as compactly supported functions and the Lorentzian function. We find that the tails decrease relatively slowly, as exponentials of fractional powers, in agreement with previous work using the moments of the distribution. Our results lead additional support to the conclusion that large vacuum stress tensor fluctuations are more probable than large thermal fluctuations, and may have observable effects.

Acknowledgments

I would like to thank my beloved parents Dino José Schiappacasse Olmos and María Angélica Cocio Ortiz. Since I was a child, they tried to give me the best possible education, the strongest values, and the warmest love. They taught me everything that I know about important things in life: sacrifice, love, and destiny. Thanks to them, today I can look at the horizon feeling I have a chance to find a smiling God at the end.

I would like to thank my academic and thesis supervisor, Professor Lawrence Ford, for the guidance, encouragement, and advice he has given me throughout my time as his student. Without doubt, I will miss so much his warm invitations to celebrate Thanksgiving in his home.

I would like to thank Professor Mark Hertzberg, for the great ideas, endless enthusiasm, and outstanding physics intuition he has shared with me during the development of our research lines. I will miss our fruitful discussions in which we could easily spend five hours.

I would like to thank myself for giving me the chance to discover myself by listening my conscious as well as my unconscious. "The sharp edge of a razor is difficult to pass over; thus the wise say the path to *enlightenment* is hard" (Katha Upanishad).

Contents

List of Tables

List of Figures

Chapter 1

Introduction and background

The definition and the use of the expectation value of a quantum stress tensor operator have been a topic of intense study in recent decades. The semiclassical theory for gravity uses the renormalized expectation value of the quantum matter stress tensor to give an approximate description of the effects of quantum matter fields on the gravitational field. As in the semiclassical theory of electromagnetic radiation, it is expected that this theory is a reasonable approximation to a more complete quantum theory of gravity coupled to matter fields. It is known that a renormalized stress energy operator for quantum fields in curved spacetime is associated with quantum corrections to Einstein's equations, via higher order derivative terms [1]. These corrections lead to physical effects, such as small scale factor oscillations around an expanding background universe and quantum particle creation [2]. Moreover, this theory has been successful about giving a plausible description of the back reaction to black hole evaporation through Hawking radiation [3]. However, the semiclassical theory does not consider the quantum fluctuations of the stress tensor around its expectation value and their possible effects. Several authors have studied a variety of physical effects associated with quantum stress tensor fluctuations. These effects include, for example, potentially observable gravity waves from quantum stress tensor fluctuations in inflationary models [4], effects of vacuum electric field fluctuations on light propagation in nonlinear materials [5, 6], and barrier penetration of charged or polarizable particles through large vacuum radiation pressure fluctuations [7, 8].

In general, the physical effects of large fluctuations of a quantum stress ten-

sor operator can be studied through the analysis of the probability distribution for the time or spacetime averaged operator. This probability distribution can be inferred (at least qualitatively) from the moments of the averaged operator, and the exact distribution was found in a two-dimensional model in Ref. [9]. The moments method was used in Ref. [10] to infer the probability distribution for several normal-ordered quadratic operators in four dimensional Minkowski spacetime with Lorentzian time averaging. These included the square of the electric field and the energy densities of a massless scalar field and of the electromagnetic field. This idea was extended in Ref. [11] to compactly supported functions of time. These results predict an asymptotic form of the probability distribution function for large fluctuations of

$$P(x) \sim c_0 x^b e^{-a x^c}\,, \quad x \gg 1\,. \tag{1.1}$$

Here the variable x is a dimensionless measure of the stress tensor, and c_0, a, b, and c are constants which depend on the sampling function. In the case of the Lorentzian time averaged electromagnetic energy density, for example, $a \sim 1$ and $c = 1/3$. Because thermal fluctuations are exponentially suppressed in energy, vacuum fluctuations can dominate over thermal fluctuations at large energies. However, the moments a_n of a quantum stress tensor operator grow very rapidly, to the extent that they might not uniquely determine the probability distribution, so it is desirable to seek alternative methods. The uniqueness of a probability distribution $P(x)$ associated with moments a_n can be analyzed using the Hamburger moment theorem [12]. This theorem states that a probability distribution with moments a_n is unique if there exist constants U and Q such that

$$|a_n| \leq U Q^n n!\,, \quad \text{for all } n\,. \tag{1.2}$$

Since this is a sufficient, but not necessary, condition for uniqueness, when Eq. (1.2) is not satisfied, the uniqueness of $P(x)$ is not totally ruled out but it is not guaranteed either. In the example above, moments of the Lorentzian time averaged electromagnetic energy density grow as $a_n \sim (3n)!$ for large n, which does not satisfy the criteria of Eq. (1.2).

In this thesis, we develop such an independent test of the moments approach for the study the probability distribution of time-averaged quantum stress tensor operators. The main idea is to diagonalize the time-averaged operator through a change of basis and calculate the cumulative probability distribution function of its quantum fluctuations in the vacuum state. We are

interested in checking the behavior predicted by the high moments approach, and in determining which modes and particle numbers give the dominant contribution to the large fluctuations. Unlike the moments approach, which primarily gives information about the asymptotic behavior of the probability distribution for large vacuum stress tensor fluctuations, the diagonalization approach in principle gives a unique probability distribution for a broad range of fluctuations x. We take the normal ordered square of the time derivative of a massless scalar field in Minkowski spacetime as our stress tensor operator, and find the tail of the probability distribution for different temporal sampling functions, specifically a class of compactly supported functions and the Lorentzian function. The tails decrease relatively slowly, as exponentials of fractional powers, in agreement with previous results using the moments of the distribution. Our results lend additional support to the conclusion that large vacuum stress tensor fluctuations are more probable than large thermal fluctuations, and may have observable effects.

This thesis is organized as follows: In Secs. 1.1 and 1.2, we briefly review the semiclassical theory of gravity and main results of Refs. [9, 10, 11] on quantum inequalities and the high moments approach to the analysis of the probability distribution for quantum stress tensor operators. In Sec. 1.3, we review fluctuations of the gravitation field as a natural extension of semiclassical gravity making focus on passive fluctuations and results from Refs. [6] and [8]. In Chap. 2, we develop an independent approach to the study of probability distributions based on the diagonalization of the operator. In Chap. 3, we show the numerical results obtained for different time sampling functions. In Chap. 4, we summarize and discuss the main results of this thesis. Chapters 2, 3, and 4 are entirely based on one of my papers published in Physical Review D **97**, 025013 (2018) [13]. Units in which $G = \hbar = c = 1$ are used throughout this thesis.

1.1 Beyond Semiclassical Gravity

The semiclassical theory of gravity considers a classical gravitational field coupled to quantum matter fields. These quantum matter fields propagate according to the theory of quantum fields in curved spacetime. In this theory the spacetime is classical but dynamical. The semiclassical Einstein Equations relate the expectation value of the stress energy momentum tensor operator

of the matter fields, $T_{\mu\nu}$, and the curvature of the spacetime as

$$G_{\mu\nu} = 8\pi\langle T_{\mu\nu}\rangle \,. \tag{1.3}$$

Here $G_{\mu\nu}$ is the Einstein tensor. The expectation value of the matter field stress tensor is obtained after a suitable regularization and renormalization processes [14]. The semiclassical theory of gravity is analogous to the semiclassical theory of electrodynamics in which the classical electromagnetic field is coupled to the expectation value of the electric current operator. We expect this semiclassical theory of gravity can approximately describe the effects of quantum matter fields upon the gravitational field on length scales well above the Planck scale and when fluctuations of $T_{\mu\nu}$ are small.

One of the greatest successes of semiclassical gravity has been the so-called Hawking effect [15], which connects thermodynamics, gravity, and quantum field theory to explain the black hole physics. Observers far from a black hole are able to see a flux of thermal radiation, Hawking radiation, which is emitted from the black hole at a temperature proportional to its surface gravity. The outgoing radiation is explained by quantum particle creation phenomena in a region outside of the event horizon. Since this radiation carries away energy and entropy from the black hole, the mass of the black hole slowly decreases leading to an eventual evaporation. Indeed, any primordial black hole with a mass less than about 10^{15} g would have evaporated by now. As long as the mass of the black hole is large compared to the Planck mass 10^{-5} g, the semiclassical Einstein equation, Eq. (1.3), gives a reasonable description of the back reaction to black hole evaporation through Hawking radiation.

On the other hand, the semiclassical theory of gravity has been successfully applied during the early Universe at scales when quantum effects are important but still far away from Planck scale. For example, quantum creation of particles is expected in an expanding universe as was first discussed by Parker [16]. Indeed, after the end of inflation, quantum creation of particles could significantly contribute to the matter and radiation of the universe [17]. In addition, quantum fluctuations during the inflationary epoch are the origin of the density perturbations which would lead to galaxies formation at later times [18]. This striking prediction seems to agree with observations coming from the cosmic microwave background radiation [19].

We have seen that the semiclassical theory of gravity provides a crucial link between the purely classical theory and a more complete quantum theory

of gravity. As was mentioned before, this theory offers us a very rich pool of physical effects which are not found at the classical level, including but not limited to black hole evaporation and cosmological particle creation.

The simplest extension of the semiclassical theory is given by considering fluctuations of the gravitation field. These kind of fluctuations can be produced by the quantum nature of gravity itself or by quantum fluctuations of the stress tensor. While the first case is known as active fluctuations, the second case is known as passive fluctuations. Here we have to point out that the inclusion of fluctuations in Eq. (1.3) to go beyond semiclassical gravity requires that these fluctuations be small [20, 21].

Active fluctuations correspond to fluctuations of gravity itself, which can be seen as fluctuations of spacetime leading to Brownian motion of test particles. If we consider photons as test particles, then gravity fluctuations lead to fluctuations of lightcones. This remarkable prediction introduces, for example, variations in arrival times of pulses from a source. Spacetime fluctuations can arise from a bath of gravitons in a nonclassical state (such as a squeezed vacuum state) [22, 23]. Note that since a black hole horizon is only a special case of a lightcone, we expect horizon fluctuations coming from spacetime geometry fluctuations. Horizon fluctuations could potentially alter the semiclassical derivation of black hole evaporation as well as allow information escapes out from black holes. Quantum fluctuations of horizons in a Schwarzschild spacetime are studied in Ref. [24] within the frame of linearized quantum gravity. These authors estimate that black hole horizon fluctuations are much smaller than Planck dimensions for black holes whose mass exceeds the Planck mass and are sufficiently small as not to invalidate the semiclassical derivation of the Hawking process. However, Refs. [25] and [26] claim that black hole horizon fluctuations are much larger. While large horizon fluctuations in Ref. [25] come from the effect on the Schwarzschild metric of mass fluctuations near the horizon, those fluctuations in Ref. [26] arise from thermal fluctuations of particles near the horizon in large angular momentum modes. In any case, black hole horizon fluctuations is an area of ongoing work which must still be deeply investigated and criticized.

Passive fluctuations are driven by quantum stress tensor fluctuations. Several authors have studied possible effects associated with these quantum fluctuations, such as luminosity fluctuations and angular blurring of astrophysical images coming from distant sources seen through a fluctuating spacetime filled with a thermal bath [27], quantum stress fluctuations of a conformally invariant field in inflationary cosmology [28], cosmological density perturbations

through passive fluctuations of the inflaton driven as a consequence of coupling between the inflaton with other massive quantum fields [29], and gravity waves in inflationary models generated by quantum stress tensor fluctuations of a conformal field [4].

Since in this thesis we are specifically interesting in quantum stress tensor fluctuations, we will review in the following sections main results in the literature on quantum inequalities and high moments approach to study large vacuum stress tensor fluctuations.

1.2 Review of previous results

Vacuum fluctuations of averaged linear quantum field operators, such as the time averaged quantum electric field, are associated with Gaussian probability distributions. The averaging can be carried out along a timelike curve, over a spatial volume, or over a spacetime volume. Let us consider a temporal averaging of a normal-ordered field operator $\chi(t, \mathbf{r})$ as follows

$$\overline{\chi} = \int_{-\infty}^{\infty} :\chi(t, \mathbf{r}): f(t) dt \,. \tag{1.4}$$

Here $\overline{\chi}$ is the time averaged field operator and $f(t)$ is the real-valued temporal sampling function with a characteristic width τ. This function must satisfy the normalization condition

$$\int_{-\infty}^{\infty} f(t) dt = 1 \,. \tag{1.5}$$

Define the nth moment of the averaged field operator in the vacuum state as

$$\mu_n = \langle 0 | (\overline{\chi})^n | 0 \rangle \,. \tag{1.6}$$

The moments are finite and uniquely define a Gaussian probability distribution as [11]

$$P(\overline{\chi}) = \frac{1}{\sqrt{2\pi\sigma}} e^{-\overline{\chi}^2/(2\sigma)} \,, \tag{1.7}$$

where $\sigma = \mu_2$ corresponds to the variance of the distribution. It depends on

the functional form of the sampling function and its width. The $\overline{\chi}^2$ dependence in the exponential of Eq. (1.7) indicates that large field fluctuations are not too likely.

On the contrary, the probability distributions for quadratic operators, such as the energy density or other components of quantum stress tensor operators, show that large vacuum quantum fluctuations are more likely than one might have expected. For example, Ref. [11] showed that normal-ordered quadratic operators in a four-dimensional Minkowski spacetime and sampled in time using compactly supported functions, have a tail for their probability distributions given by Eq. (1.1). The tail decrease relatively slowly, as exponentials of fractional powers, in comparison to a Gaussian distribution.

1.2.1 Quantum Inequalities

Quantum inequalities set lower bounds on the expectation values of smeared quantum stress tensor components in arbitrary quantum states. For the case of a two-dimensional spacetime, the sampling may be carried out over space, time, or spacetime. But for the case of a four-dimensional spacetime, there are no quantum inequalities when the sampling is only carried out over space [30].

The weak energy condition imposes over the stress-energy tensor $T_{\mu\nu}$ the inequality $T_{ab}u^a u^b \geq 0$ for all timelike vector u^a. All known forms of classical matters obey this condition. By contrast, this condition is violated in quantum field theory where the renormalized energy density may take arbitrarily negative values at points of spacetime [31]. Quantum inequalities impose strong constraints over negative values that can be reachable by energy densities. Without these restrictions, a number of bizarre possibilities such as traversable wormholes [32], faster-than-light travel [33], time travel [32, 34], and violations of the second law of thermodynamics [35], would be possible.

In four spacetime dimensions, a general quantum inequality for a massless scalar field involving a temporal sampling takes the form [20, 35, 36, 37, 38]

$$\int_{-\infty}^{\infty} \langle{:}T_{tt}(t,0){:}\rangle g(t) \geq -\frac{C}{\tau^4}\,, \tag{1.8}$$

where $\langle{:}T_{tt}(t,0){:}\rangle$ is the renormalized energy density in an arbitrary quantum state measured by an stationary observer at the spatial origin and $g(t)$ is a non-negative sampling function with characteristic width τ. Here C is a numerical

constant which is typically small compared to unity. The specific value of C depends on the form of the sampling function but not its width. Equation (1.8) tells us that the magnitude and the fourth power of the duration of the negative energy density are inversely proportional. Suppose that an observer measures a pulse of negative energy density with a magnitude of ρ_m during a period of time of τ, then the observer must measure $\rho_m < 1/\tau^4$.

There is a very deep connection between quantum inequality bounds and the probability distribution for quantum stress tensor fluctuations in the vacuum. Quantum inequality bounds set lower bounds on the expectation values of sampled stress tensors in arbitrary physically reasonable quantum states. A quantum inequality bound corresponds to the lowest eigenvalue associated with a sampled operator, and is therefore the smallest result which one can find in a measurement. These bounds are also the lower bounds of the support of the respective probability distributions in the vacuum state (for a rigorous explanation, see [18] in Ref. [9].)

1.2.2 Shifted Gamma Distribution

Here we review the main results of Ref. [9]. Consider a general unitary, positive energy conformal field theory in a two-dimensional Minkowski spacetime with central charge c. For the case of a massless scalar field, for example, the central charge is equal to one. Define the time average of the energy density operator $T_{tt}(t,0)$ with a Gaussian function as

$$\overline{\rho} = \frac{1}{\sqrt{\pi}\tau} \int_{-\infty}^{\infty} :T_{tt}(t,0): e^{-t^2/\tau^2} dt \,, \tag{1.9}$$

where τ is a characteristic width. The probability distribution associated with measurements in the vacuum state of the Gaussian sampled energy density is obtained by finding a closed expression for the generating function of the nth moments of Eq. 1.9, $\langle 0|(\overline{\rho})^n|0\rangle$, from which the underlying probability distribution can be derived. Defining the dimensionless variable $x \equiv \overline{\rho}\tau^2$, the probability distribution $P(x)$ is given by a shifted Gamma function according to

$$P(x) = \mathcal{H}(x + x_0) \frac{\beta^\alpha (x + x_0)^{\alpha - 1}}{\Gamma(\alpha)} e^{-\pi(x + x_0)} \,, \tag{1.10}$$

where $\mathcal{H}$ is the Heaviside function, $x_0 = c/(12\pi)$, $\alpha = c/12$, and $\beta = \pi$. There is a lower bound of the distribution given by $x = -x_0$. For the case of a mass-

less scalar field, the lower bound is exactly the same as the optimum lower bound coming from the respective quantum inequality [40]. As was mentioned before, quantum inequalities bounds and stress tensor probability distributions are deeply connected. On the contrary, there is no upper bound on the support of $P(x)$. So any arbitrary large value of the energy density can be reached by vacuum fluctuations.

Using Eq. (1.10) and the binomial theorem, the nth moment of $P(x)$ can be expressed in closed form as a generalized hypergeometrc function ${}_2F_0$ as follows

$$a_n = \int_{-x_0}^{\infty} x^n P(x) dx = (-x_0)^n \, {}_2F_0 \left(\alpha, -n; \frac{1}{\beta x_0} \right) . \tag{1.11}$$

For large n, $a_n \sim n!$ satisfying the sufficient criteria for uniqueness of $P(x)$, Eq. (1.10), given by the Hamburger moment theorem, Eq. (1.2).

The shifted Gamma function of Eq. (1.10) also appears in the analysis of probability distributions in a four-dimensional spacetime. Let us consider a massless scalar field φ. Take the normal-ordered time-averaged quadratic operator $\overline{\varphi^2}$ as

$$\overline{\varphi^2} = \int_{-\infty}^{\infty} :\varphi^2(t,0): f_L(t) \, , \quad \text{with} \;\; f_L(t) = \frac{\tau}{\pi(t^2+\tau^2)} \, , \tag{1.12}$$

where $f_L(t)$ is a Lorentzian function with characteristic width τ. Define the dimensionless variable $x \equiv (4\pi\tau)^2 \overline{\varphi^2}$. After explicit calculations of the first three moments of the quadratic operator defined by $\langle 0|(\overline{\varphi^2})^n|0\rangle$, determine free parameters in Eq. (1.11) by a fitting procedure to obtain $\alpha = 1/72$, $\beta = 1/12$, and $x_0 = 1/6$. The resultant fitted form of the probability distribution remarkably matches the subsequent moments exactly through a_{57} (see Table I in Ref. [9] for the first eight moments). As before, the probability distribution does not have an upper bound but there is a lower bound of the distribution given by $x = -x_0$.

The probability distribution for both cases, namely, the time average of the normal-ordered energy density operator in two-dimensional Minkowski spacetime and the time average of the square of the massless scalar field in four-dimensional Minkowski spacetime, is uniquely defined by its moments. As was mentioned above, the moments of the shifted Gamma distribution fulfill the sufficient criteria for uniqueness given by the Hamburger moment theorem, Eq. 1.2.

1.2.3 Probability distributions in four dimensions

Working in four-dimensional Minkowski spacetime, let $S(t, \mathbf{r})$ be an operator which is a quadratic function of a free field operator and define its time average with a real-valued sampling function $f(t)$ by

$$\overline{S} = \int_{-\infty}^{\infty} :S(t, \mathbf{r}): f(t) dt \,. \tag{1.13}$$

We will consider measurements of the time average $\overline{S}$ rather than S. The sampling function has a characteristic width τ and should decay quickly as $|t| \gg \tau$. The sampling function can be, for example, a Lorentzian function or compactly supported functions. For any given sampling function $f(t)$ define the nth moment of the normal-ordered time-averaged quadratic operator $\overline{S}$, Eq. (1.13), as

$$\mu_n = \langle 0 | (\overline{S})^n | 0 \rangle \,, \tag{1.14}$$

where $|0\rangle$ is the Minkowski vacuum state of the theory. As we will see later, the form of the Fourier transform $\hat{f}$ defines the rate of growth of the moments μ_n and, as a result, the probability for large fluctuations.

In Ref. [10], the probability distributions in a four-dimensional Minkowski spacetime were analyzed for several normal-ordered quadratic operators, such as the square of the time derivative of a free massless scalar field or the square of the electric field strength, using a Lorentzian function as a sampling function in time. Reference [11] analyzes the probability distributions of normal-ordered quadratic operators in four-dimensional Minkowski spacetime using compactly supported functions in time. We will review in detail the main results of both references.

1.2.4 Lorentzian temporal sampling function

Here we review the main results of Ref. [10]. In Eq. (1.13), take the sampling function to be a Lorentzian function, $f_L(t)$, according to

$$f_L(t) = \frac{\tau}{\pi(t^2 + \tau^2)} \,, \tag{1.15}$$

whose Fourier transformation, $\hat{f}_L(\omega)$, and normalization are given by

$$\hat{f}_L(\omega) = \int_{-\infty}^{\infty} dt\, e^{-i\omega t} f_L(t) = e^{-|\omega\tau|}\,, \text{ and } \hat{f}_L(0) = 1\,. \tag{1.16}$$

Here τ is the characteristic width of $f_L(t)$.

In Eq. (1.13), take as quadratic operators the square of the time derivative of a free massless scalar field, $\dot{\varphi}^2$, the square of the electric field strength, E^2, and the energy densities of the scalar and electromagnetic fields, ρ_φ and $\rho_{\rm EM}$, respectively. In four dimensions, all these operators have dimensions of length^{-4}. Define the dimensionless variable $x = (4\pi\tau^2)^2\overline{S}$, where $\overline{S}$ is the Lorentzian time average of $(\dot{\varphi}^2, E^2, \rho_\varphi, \rho_{\rm EM}\ )$ according to Eq. (1.13). If $P(x)$ is the probability distribution for each one of these cases, then the nth moment of $P(x)$ is given by

$$a_n = \int_{-x_0}^{\infty} x^n P(x) dx\,, \tag{1.17}$$

where $-x_0$ is the lower bound of the distribution. We can relate the nth moment of $P(x)$ with Eq. (1.14) as

$$\mu_n = (4\pi\tau^2)^{-2n} a_n = (4\pi\tau)^{-2n} \int_{-x_0}^{\infty} x^n P(x) dx\,. \tag{1.18}$$

Here μ_n is formed by the vacuum expectation value of n copies of the sampled normal-ordered quadratic operator according to

$$\mu_n = \int_{-\infty}^{\infty} dt_1 f_L(t_1) \int_{-\infty}^{\infty} dt_2 f_L(t_2) ... \int_{-\infty}^{\infty} dt_n f_L(t_n) \langle 0| :S_1::S_2:...:S_n:|0\rangle\,, \tag{1.19}$$

where $S_j = S(t_j, \mathbf{r})$. For the sake of simplicity, suppose that $\dot{\varphi}^2$ is the quadratic operator in consideration and $\dot{\varphi}_j$ is the field at time t_j. The Wick's theorem tells us that the respective nth moment of the sampled operator can be calculated as the sum of all possible contractions of the form

$$\dot{\varphi}_1\dot{\varphi}_1\dot{\varphi}_2\dot{\varphi}_2\dot{\varphi}_3\dot{\varphi}_3 ... \dot{\varphi}_n\dot{\varphi}_n\,, \tag{1.20}$$

where any $\dot{\varphi}_i$ is contracted with a $\dot{\varphi}_j$ but $i \neq j$ in each contraction. These contractions can be represented by graphs with n vertices where every vertex is met by two lines. Every line from $\dot{\varphi}_i$ to $\dot{\varphi}_j$ represents a contraction. For

example, for $n \geq 2$ only two contractions contribute to the second moment as is shown by Fig. 1.1. For $n \geq 4$, the Wick expansion includes connected as

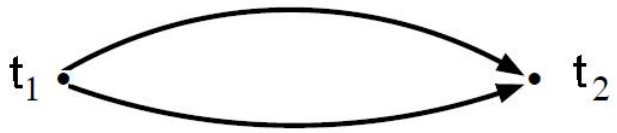

Figure 1.1: Graphs for $n = 2$. Every line represents a contractions between two $\dot{\varphi}_i$. (Figure taken from Ref. [10].)

well as disconnected graphs. We define the full moment generating function, $M(\lambda)$, as

$$M(\lambda) = \sum_{n=0}^{\infty} \frac{\lambda^n a_n}{n!}\,, \tag{1.21}$$

where λ is the parameter of expansion. The nth moment of the probability distribution can be expressed by

$$a_n = \left(\frac{d^n M}{d\lambda^n}\right)_{\lambda=0}\,. \tag{1.22}$$

In a similar way, we can define the connected moment generating function, W, with the same form as Eq. (1.21). This function generates moments which arise from considering only connected graphs. Note that as M is the exponential of W, there is no need to take into account disconnected graphs explicitly.

The procedure to calculate the first N moments a_n is the following. Compute explicitly N connected moments. W can be approximated by a Nth degree polynomial in λ. Using $M = \exp(W)$, the full moment generating function can be calculated. If M is also approximated by a Nth degree polynomial in λ, the first N moments of a_n may be extracted as the coefficients of this polynomial.

For $n \gg 1$, the nth moment of the probability distribution for all quadratic operators mentioned here has an asymptotic form given by

$$a_n \sim C D^n (3n-4)!\,, \tag{1.23}$$

where C and D are numerical constants. Note that this asymptotic form for the moments does not satisfy the sufficient criteria for uniqueness given by the Hamburger condition, Eq. (1.2).

Based on the knowledge of a finite number of moments a_n, Eq. (1.17) , we can obtain an approximate estimate of the lower bound $-x_0$ of a probability distribution $P(x)$ with moments a_n and support bounded below by $-x_0$ (this technique is known as Stieltjes moment test). Here we proceed to summarize Sec. IV of Ref. [10]. Consider the expression

$$I(y) = \int_{-x_0}^{\infty} (x+y)|q(x)|^2 P(x)dx\,, \tag{1.24}$$

where $y \geq x_0$ and $q(x)$ is a polynomial. Define this polynomial as

$$q(x) = \sum_{n=0}^{N-1} \beta_n x^n\,, \tag{1.25}$$

and replace it into Eq. (1.24) to obtain

$$I(Y) = \sum_{m,n=0}^{N-1} M_{m,n}(N,y)\beta_m^*\beta_n \geq 0\,. \tag{1.26}$$

Here $M(N,y)$ is a real symmetric $N\times N$ matrix whose elements are determined by the moments according to

$$M_{m,n}(N,y) = a_{m+n+1} + y\, a_{m+n} \quad \text{with } 0 \leq m,n \leq N-1\,. \tag{1.27}$$

If β_n are the components of an eigenvector of M with eigenvalue λ, we have

$$\sum_{n=0}^{N-1} M_{mn}(N,y)\beta_n = \lambda\beta_m\,, \tag{1.28}$$

$$I(y) = \lambda \sum_{m=0}^{N-1} |\beta_m|^2\,. \tag{1.29}$$

Here $M(N,y)$ is a positive semidefinite matrix for all N and $y \geq x_0$. When y decreases below x_0, $M(N,y)$ can show negative eigenvalues. Let y_N be the lowest value of y at which $M(N,y) \geq 0$ is still true. In practical terms, y_N is the largest root of the Nth degree polynomial equation given by $\det M(N,y) = 0$.

Since $y_{N+1} \geq y_N$, the sequence in N converges as

$$y_\infty = \lim_{N\to\infty} y_N \leq x_0 \,. \tag{1.30}$$

If y_∞ is a finite number, then for any probability distribution $\tilde{P}(x)$ with the same moments a_n and whose support is bounded from bellow by $-\tilde{x}_0$, the condition $y_\infty \leq -\tilde{x}_0$ will be true. Consider the specific case of the quadratic operator $\dot{\varphi}^2$, then a set of values of $y_N(\dot{\varphi}^2)$ can be calculated (see Table II in Ref. [9]). The difference between successive terms, $y_{N+1}(\dot{\varphi}^2) - y_N(\dot{\varphi}^2)$, decays as $O(N^{-3/2})$. The set of values of $y_N(\dot{\varphi}^2)$ can be fitted to a trial function $y_N(\dot{\varphi}^2) = a + b\,N^{-1/2} + c\,N^{-1} + d\,N^{-3/2}$ using a least square method. The resulting formula for values $y_{21} \leq y_N \leq y_{33}$ is given by

$$y_N(\dot{\varphi}^2) \approx 0.023618 - \frac{0.012426}{N^{1/2}} - \frac{0.0027684}{N} - \frac{0.0065339}{N^{3/2}} \,. \tag{1.31}$$

Here coefficients have been rounded until the fifth significant digit.

A similar procedure can be applied to obtain an estimate of a lower bound for others operators such as E^2, ρ_φ, and $\rho_{\rm EM}$. However, relations between the moment generating functions of these operators can be used to relate the respective lower bounds of their probability distributions. Following this last procedure, estimates of the lower bounds of the probability distributions of the mentioned operators are given by

$$-x_0(\dot{\varphi}^2) = -x_0(\rho_\varphi) = -(1/2)x_0(\rho_{EM}) = -(1/2)x_0(E^2) \approx -0.0236 \,. \tag{1.32}$$

These estimates of lower bounds can be also considered as estimates of the respective optimal quantum inequality bounds.

From the knowledge of a finite set of moments a_n, we can also obtain valuable information for the tail of the associated probability distribution. Consider the following ansatz for $P(x)$ when $x \gg 1$:

$$P(x) \sim c_0\, x^b\, e^{-a\, x^c} \,, \tag{1.33}$$

where a, b, c, and c_0 are constants to be determined. Replace this expression

into Eq. (1.17). Then large moments behavior for $n \gg 1$ are given by

$$a_n = \int_{-x_0}^{\infty} x^n P(x) dx \approx c_0 \int_0^{\infty} x^{n+b} e^{-ax^c} , \tag{1.34}$$

$$a_n \approx \frac{c_0\, a^{-(n+b+1)/c}}{c} \left[(n+b+1)/c - 1\right]! , \tag{1.35}$$

where we have replaced $-x_0$ by 0 as the lower limit of the second integral in Eq. (1.34), since the main contribution to the integral comes from $x \gg 1$. Matching this equation with the asymptotic form for large moments of Eq. (1.23), we can express constants a, b, c, and c_0 in function of constants C and D as

$$a = D^{-1/3} , \;\; b = -2, \;\; c = 1/3 , \;\; c_0 = C\, D/3 . \tag{1.36}$$

Replace values for b and c in Eq. (1.35) and calculate the ratio between two successive moments to obtain

$$\frac{a_{n+1}}{a_n} \approx \frac{3(n-1)(3n-2)(3n-1)}{a^3} . \tag{1.37}$$

Using the previous set of computed values for moments a_n (see Table II in Ref. [9]), the value for a can be found for each quadratic operator. Knowing values for a, b, and c, the value for c_0 can be found using Eq. (1.35). For the ansatz given by Eq. (1.33), values of the parameters for the different quadratic operators considered in the present analysis are shown by Table 1.1.

Table 1.1: Numerical values of the parameters of the tail of the probability distribution according to Eq. (1.33).

Operator	$\boldsymbol{c_0}$	$\boldsymbol{a}$	$\boldsymbol{b}$	$\boldsymbol{c}$
$\boldsymbol{\dot{\varphi}^2}$	0.47769605	0.6677494904	-2	1/3
$\mathbf{E^2}$	0.95539211	0.7643823521	-2	1/3
$\boldsymbol{\rho_{\varphi}}$	0.23884802	0.8413116390	-2	1/3
$\boldsymbol{\rho_{\mathrm{EM}}}$	0.95539211	0.9630614156	-2	1/3

1.2.5 Compactly supported functions

Here we review the main results of Ref. [11]. Let us consider the time average of a quadratic operator with a sampling function $f(t)$, Eq. (1.13). Since the measurement of the operator occurs in a finite interval of time, the sampling function is better described by a smooth and compactly supported function rather than a non-compactly supported sampling function. This kind of sampling function is strictly zero outside a finite region, avoiding the long temporal tails of functions like the Lorentzian. It therefore gives a better description of a measurement which begins and ends at finite times. Take the sampling function in Eq. (1.13) to be a compactly supported nonnegative functions, $f_{\rm cs}(t)$, whose Fourier transform has the following asymptotic form when $\omega\tau \gg 1$:

$$\hat{f}_{\rm cs}(\omega) \sim \gamma\, e^{-\beta|\omega\tau|^{\alpha}}\,, \tag{1.38}$$

where α, γ, and β are constants. Here $\alpha \in (0,1)$ is a decay parameter which defines the rate of decrease of $\hat{f}_{\rm cs}(\omega)$ (values $\alpha \geq 1$ are incompatible with $f_{\rm cs}$ having compact support). It is worth emphasizing that τ does not directly measure the support of $f_{\rm cs}$, but rather indicates the shortest characteristic timescale associated with $f_{\rm cs}$; in our examples, this will characterize the switch-on and switch-off regions. Setting the initial switch-on to occur at $t = 0$, the asymptotic form of $f_{\rm cs}(t)$ at $t \to 0^{+}$ depends on the decay parameter as follows

$$f_{\rm cs}(t) \sim w_4 t^{-w_1} e^{-w_2\ t^{-w_3}} \tag{1.39}$$

where

$$w_1 = \frac{2-\alpha}{2-2\alpha}\,, \tag{1.40}$$

$$w_2 = (1-\alpha)\alpha^{\alpha/(1-\alpha)}\,, \tag{1.41}$$

$$w_3 = \frac{\alpha}{1-\alpha}\,, \tag{1.42}$$

$$w_4 = \frac{\alpha^{1/(2-2\alpha)}}{\sqrt{2\pi(1-\alpha)}}\,. \tag{1.43}$$

The asymptotic form of $f_{\rm cs}(t)$ at the switch-off is the same. Equations (1.38) and (1.39) show that the decay parameter determines both the rate of decrease of the asymptotic form of $\hat{f}_{\rm cs}(\omega)$ and the behavior of $f_{\rm cs}(t)$ at the switch-on

and switch-off regions. A simple electrical circuit can be built setting $\alpha = 1/2$ to obtain $f(t) \sim (1/\sqrt{4\pi})\ t^{-3/2} e^{-1/(4t)}$ at $t \to 0^+$.

For any given compactly supported function $f_{\rm cs}(t)$, we still define the nth moment of the normal-ordered time-averaged quadratic operator $\overline{S}$, Eq. (1.13), to be given by Eq. (1.14).

In the first instance, we work in a box of finite volume and express $\overline{S}$ in a mode sum of creation and annihilation bosonic operators as

$$\overline{S} = \sum_{ij} \left(\tilde{A}_{ij} a_i^\dagger a_j + \tilde{B}_{ij} a_i a_j + \tilde{B}^*_{ij} a_i^\dagger a_j^\dagger \right) , \tag{1.44}$$

where $\tilde{A}_{ij}$ and $\tilde{B}_{ij}$ are components of symmetric matrices $\tilde{A}$ and $\tilde{B}$, which have the functional forms

$$\tilde{A}_{ij} \propto (\omega_i \omega_j)^{1/2} \hat{f}_{\rm cs}(\omega_i - \omega_j) , \tag{1.45}$$

$$\tilde{B}_{ij} \propto (\omega_i \omega_j)^{1/2} \hat{f}_{\rm cs}(\omega_i + \omega_j) , \tag{1.46}$$

where ω_i are the mode frequencies. Precise forms of $\tilde{A}$ and $\tilde{B}$ will be given when we come to specific examples in Chap. 3. The moment μ_n can be expressed as a nth degree polynomial in these components. As n increases, the number of terms in the expression for the nth moment grows rapidly. Fortunately, only one term gives the dominant contribution for $n \gg 1$:

$$M_n = 4 \sum_{j_1 \cdots j_n} \tilde{B}_{j_1 j_2} \tilde{A}_{j_2 j_3} \tilde{A}_{j_3 j_4} \cdots \tilde{A}_{j_{n-1} j_n} \tilde{B}^*_{j_n j_1} . \tag{1.47}$$

First, $\tilde{B}_{j_1 j_2}$ and $\tilde{B}^*_{j_n j_1}$ have to begin and end, respectively, the expression for M_n because $\tilde{B}^*_{ij} a_i^\dagger a_j^\dagger$ and $\tilde{B}_{ij} a_i a_j$ in Eq. (1.44) are the only terms which do not annihilate the vacuum from the left and right, respectively. Second, all the remaining coefficients in M_n are $\tilde{A}_{ij}$'s, which fall slower than $\tilde{B}_{ij}$'s when ω_i becomes large. This arises because the $\tilde{A}_{ij}$ involve a difference in frequencies, as opposed to the sum in the $\tilde{B}_{ij}$. Provided that $\hat{f}_{\rm cs} \geq 0$, all the terms contributing to the nth moment are nonnegative, so M_n is actually a lower bound on μ_n, which will gives us a lower bound on the probability distribution for large vacuum fluctuations. Here we have to mention that the same reasoning works if we use in Eqs. (1.45) and (1.46) a Lorentzian sampling function

instead of compactly supported functions. Indeed, there is numerical evidence that $\mu_n \sim M_n$ for large n using a Lorentzian sampling of the quadratic operator $:\dot{\varphi}^2:$, where φ is a massless scalar field in four-dimensional Minkowski spacetime. Using data from Table I in Ref. [10], we have $(M_4/\mu_4) \approx 0.843$, $(M_{10}/\mu_{10}) \approx 0.966$, and $(M_{20}/\mu_{20}) \approx 0.993$. The ratio (M_n/μ_n) steadily approaches to one as n increases.

Coming back to our discussion of the dominant term M_n under a compactly supported sampling function, consider the time average of $:\dot{\varphi}^2:$. Then, passing to a continuous mode sum, the dominant term takes the form

$$M_n = k_n \int_0^\infty d\omega_1 \cdots d\omega_n (\omega_1 \cdots \omega_n)^3 \times \\ \hat{f}_{\rm cs}(\omega_1 + \omega_2)\hat{f}_{\rm cs}(\omega_2 - \omega_3) \cdots \hat{f}_{\rm cs}(\omega_{n-1} - \omega_n)\hat{f}_{\rm cs}(\omega_n + \omega_1)\,, \tag{1.48}$$

where $k_n = 1/(2\pi^2)^n$. If $\hat{f}_{\rm cs}$ has the asymptotic form (1.38), then the dominant term has the asymptotic form, in units in which $\tau = 1$,

$$M_n \sim \frac{3!\gamma^2 B_0 B^n [2\pi f_{\rm cs}(0)]^{n-2} \Gamma\left[(3n+2)/\alpha - 4\right]}{(2\pi^2)^n \alpha^5 (2\beta)^{(3n+2)/\alpha}} \tag{1.49}$$

for $n \gg 1$, where $k_n = B_0 B^n$ and $f_{\rm cs}(0) = (2\pi)^{-1} \int_{-\infty}^{\infty} d\omega \hat{f}_{\rm cs}(\omega)$ (see Sec. IV of [11]). The most important part of this expression is the gamma function factor, which leads a rapid rate of growth of the high moments, $M_n \propto (3n/\alpha)!$. Thus, the parameter α is crucial in determining the rate of growth of the moments when $n \gg 1$.

The goal is to use the asymptotic form for the moments, Eq. (1.49), to obtain information about the probability distribution for large vacuum fluctuations. Return to arbitrary units for the characteristic timescale τ. Let $P(x)$ be the probability density for the distribution of the dimensionless variable $x = \overline{S}\tau^4$ in measurements of $\overline{S}$ in the vacuum state. While there is no upper bound on the values of x that can arise – and therefore no upper bound on the support of P – there is a lower bound $x > -x_0$ for some $x_0 > 0$. As was mentioned before in Sec. 1.2.1, there is a deep connection between this feature of the stress tensor probability distribution and quantum inequality bounds. We define the tail distribution (also called the complementary cumulative distribution function), $P_>(x)$, as the probability of finding any value $y \geq x$ in a

measurement

$$P_>(x) = \int_x^\infty P(y)dy \tag{1.50}$$

and of course P is normalized so that $P_>(x) = 1$ for $x \leq -x_0$. The nth moment of $\overline{S}$ can be written in terms of P as

$$\mu_n = \tau^{-4n} \int_{-x_0}^\infty x^n P(x)\, dx \tag{1.51}$$

and this can be compared with the asymptotic form of the dominant contribution M_n, Eq. (1.49), to infer information about $P(x)$ and $P_>(x)$. In this way, we are led to consider the asymptotic forms

$$P(x) \sim c_0 x^b e^{-ax^c}\,, \quad \text{and} \quad P_>(x) \sim \frac{c_0 a^{-(1+b)/c}}{c} \Gamma\left(\frac{1+b}{c}, ax^c\right)\,, \tag{1.52}$$

for large vacuum fluctuations, $x \gg 1$, where c_0, a, b, and c are constants to be determined, and for which the corresponding moments obey

$$\mu_n \approx c_0 \int_{-x_0}^\infty x^{n+b} e^{-ax^c} dx = \frac{c_0}{c} a^{-(n+b+1)/c}\, \Gamma[(n+b+1)/c]\,. \tag{1.53}$$

when n becomes large. The similarity between this expression and the asymptotic form for M_n, Eq. (1.49), is evident, and leads to the identifications

$$c = \frac{\alpha}{3}\,, \;\; b = -\frac{(4\alpha+1)}{3}\,, \;\; a = 2\beta\left[2\pi B f_{\rm cs}(0)\right]^{-\alpha/3}\,, \tag{1.54}$$

$$c_0 = c a^{(1+b)/c}\, B_0\, 3! \gamma^2 \alpha^{-5}\, (2\beta)^{-2/\alpha} [2\pi f_{\rm cs}(0)]^{-2}\,, \tag{1.55}$$

where $B = 1/(2\pi^2)$ and $B_0 = 1$. However, the situation is a little bit more subtle, because it is not guaranteed that a set of moments growing as fast as $(3n/\alpha)!$ (for $\alpha < 1$) determines a unique probability distribution [12]. Fortunately, the difference between two probability distributions with the same moments is just an oscillatory function, which does not add any interesting feature to the general form of $P(x)$ for our purposes. Therefore the parameters in Eq. (1.54) should provide a good approximation to the asymptotic behavior of $P(x)$ and $P_>(x)$. Rigorous arguments to this effect are given in Sec. VI

of [10].

The argument just given applies to the case of a compactly supported function with asymptotics given by Eq. (1.38). For the case of a non-compactly supported sampling function such as a Lorentzian, Eq. (1.16), a slightly different argument is needed to compute the asymptotic form of the dominant contribution M_n, as is explained in detail in Ref. [10]. However, the analysis of high moments still leads to an asymptotic form for $P(x)$ given by Eq. (1.52) with $c = 1/3$. This is consistent with the $\alpha \to 1$ limit of the relation $c = \alpha/3$ derived for compactly supported functions, in which limit the asymptotic form (1.38) agrees with that of the Lorentzian (1.16), with $\gamma = \beta = 1$.

In general, we see that the decay parameter α in the asymptotic form of the sampling function's Fourier transform determines the rate of decay in $P(x)$ for large x, and hence the probability of large vacuum fluctuations. The smaller α is, the more slowly the tail decreases and the greater the probability of large fluctuations becomes. For compactly supported functions, the value of α is related to the rate of switch-on and switch-off of $f_{\rm cs}(t)$. [See Eqs. (51) and (52) in Ref. [11].]

1.3 Physical effects

Since we are interesting in the study of large vacuum fluctuations of quantum stress tensor operators, we will review in detail main results of Refs. [6] and [8] about flight time variations in nonlinear dielectric materials and enhancement of barrier penetration of charged particles, respectively. Describing these results will help us to emphasize the importance of the study of passive fluctuations.

1.3.1 Flight time variations in nonlinear dielectrics

Here we briefly recall main results of Ref. [6]. Results on the vacuum probability distribution of the Lorentzian time average of the normal-ordered squared electric field operator of Ref. [10] can be used to analyze flight time variations of probe pulses in a nonlinear dielectric material.

Let us consider a probe pulse traveling through a slab of optical material. For our purposes it is enough to take the second and third order susceptibility

tensors equal to zero and nonzero but small, respectively. Take the probe pulse to be polarized in the z-direction and propagating in the x-direction. Assume that the probe field is smaller in magnitude than the external field $E_i^0(\mathbf{x},t)$ and the dispersion of the wavepacket is negligible. Then the flight time t_d of a probe pulse traveling a distance d through the material in the x-direction is given by

$$t_d = \int_0^d n_p \left[1 + \mu_{ij}\, E_j^0(\mathbf{x}, n_p x)\, E_j^0(\mathbf{x}, n_p x)\right] dx\,, \tag{1.56}$$

where

$$n_p = \sqrt{1 + \chi_{zz}^{(1)}}\,, \tag{1.57}$$

$$\mu_{ij} = \frac{3\left(\gamma_{ij} + \gamma_{ji}\right)}{4}\,, \tag{1.58}$$

$$\gamma_{ij} = \frac{\chi_{zzij}^{(3)} + \chi_{zizj}^{(3)} + \chi_{zijz}^{(3)}}{3n_p^2}\,. \tag{1.59}$$

Here $\chi_{ij}^{(1)}$ and $\chi_{ijkl}^{(3)}$ are the first and third order susceptibility tensors, respectively, n_p is the refractive index of the medium measured by the probe pulse (when only linear effects are considered), and the repeated indices are summed upon as usual. Note that we take $t = n_p x$ to evaluate the integrand in Eq. (1.56), namely, we follow the worldline of a pulse traveling at speed $1/n_p$.

Now we take $\mathbf{E^0}$ to be the quantized electric field. The flight time, Eq. (1.56), becomes an operator where the quadratic term in the external field is taken to be normal-ordered, namely, we replace $E_i^0(\mathbf{x},t)E_j^0(\mathbf{x},t)$ by $:E_i^0(\mathbf{x},t)E_j^0(\mathbf{x},t):$. Then the finite mean flight time in the vacuum state to leading order is just $\langle t_d\rangle = n_p d$. From Eq. (1.56), we see that large vacuum fluctuations associated with the normal-ordered square of the electric field strength could lead to significant flight time variations. Following results from Ref. [10] explained in Sec. 1.2.4, let $\overline{E^2}$ be the Lorentzian time average of the normal-ordered square of the electric field operator at the path followed by the probe wavepacket. Define the dimensionless variable $x = (4\pi\tau^2)^2\overline{E^2}$, where τ is the characteristic width as usual. The probability $P(x)$ of finding a given value of x in a measurement in the vacuum state has a support bounded below by $-x_0$ and moments μ_n given by Eq. (1.19). For large vacuum fluctuations, $x \gg 1$, we have time delays for the mean flight time. Using Eq. (1.33) and values from

Table 1.1, the asymptotic form of the probability distribution is approximately

$$P(x) \sim c_0\, x^{-2}\, e^{-a\, x^{1/3}}\,, \tag{1.60}$$

where $c_0 \approx 0.955$ and $a \approx 0.764$. Note that $P(x)$ decays much more slowly than a Gaussian or an exponential function. Using Eq. (1.60), we can calculate approximately the complementary cumulative probability distribution, Eq. (1.50), when $y \gg 1$ to find

$$P_{>}(y) = \int_y^\infty P(x)dx \approx \frac{3\, c_0}{a\, y^{4/3}} e^{-ay^{1/3}}\,. \tag{1.61}$$

Using the value of the second moment of $P(x)$, Eq. (1.17) with $n = 2$, we have that the root mean square of x is $x_{rms} = \sqrt{a_2} = \sqrt{6}$ (See Table I in Ref. [10]). Now we may use Eq. 1.61 to calculate the probability of finding results which largely exceeds the value of x_{rms}. For example, there is a probability of the order of 10^{-5} of finding a squared electric field fluctuation 100 times larger than the root mean square value (See Table I in Ref. [6]). As the same probabilities apply for the flight time delay produced by vacuum squared electric field fluctuations, there is a non-negligible probability that the probe pulse undergoes a potentially measurable time delay due to these fluctuations.

1.3.2 Barrier penetration of charged particles

Here we briefly recall the main results of Ref. [8]. Results on the vacuum probability distributions for normal-ordered time-averaged quantum stress tensor components using compactly supported functions of Ref. [11] can be used to analyze large vacuum radiation pressure fluctuations.

Working in a four-dimensional Minkowski spacetime, let R^{tz} be the momentum flux of the electromagnetic stress tensor in the z-direction. From Eq. (1.13), its time average with a real-valued sampling function $f(t)$ is given by

$$\overline{R^z} = \int_{-\infty}^{\infty} :R^{tz}(t, \mathbf{r}):f(t)dt\,, \tag{1.62}$$

where $:R^{tz}: = R^{tz}$ and the sampling is taken at a fixed spatial location. The asymptotic form of the Fourier transform of the sampling function $f(t)$ when $|\omega\tau| \gg 1$ is given by Eq. (1.38) with $\gamma = \beta = 1$.

The nth moment of $\overline{R^z}$ is given by $\mu_n = \langle 0|(\overline{R^z})^n|0\rangle$. When $n \gg 1$, the asymptotic form of the moments is given by Eq. (1.49) with $k_n = 4/(6\pi^2)^n$.

Let $P(x)$ be the probability density for the distribution of the dimensionless variable $x = \tau^4\overline{R^z}$ in measurements of $\overline{R^z}$ in the vacuum state. Unlike the case of the time average of $:\dot{\varphi}^2:$ analyzed in Sec. 1.2.5, there is no lower bound on the values of x and the distribution is even under the transformation $x \to -x$. The probability distribution is normalized to unity and the tail distribution, $P_>(x)$, is given by Eq. (1.50).

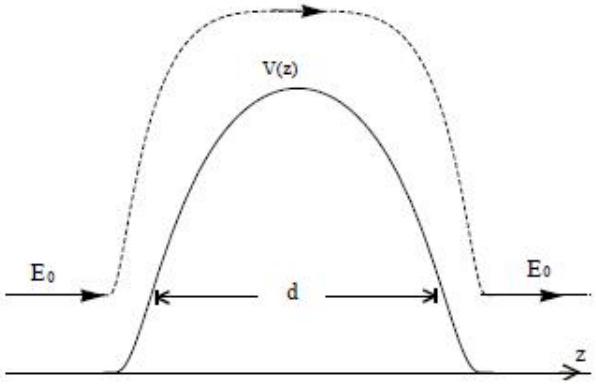

Figure 1.2: A charged particle can temporarily receive an extra energy coming from quantum radiation pressure fluctuations allowing it to fly over the potential barrier. (Figure taken from Ref. [8].)

For large vacuum fluctuations, $x \gg 1$, the asymptotic forms of $P(x)$ and $P_>(x)$ are still given by Eq. (1.52). Constants c_0, a, b, and c in those asymptotic expressions are given by Eqs. (1.54, 1.55) by taking $B_0 = 4$ and $B = 1/(6\pi^2)$. The smaller the parameter decay, α, the greater the probability of large fluctuations. Large vacuum radiation pressure fluctuations of the quantized electromagnetic field are well described by a tail of a probability distribution which fall more slowly than a Gaussian function, as exponentials of fractional powers. For this reason large vacuum radiation pressure fluctuations should have a noticeable role in several physics processes. Under some conditions, these kind of fluctuations could temporarily give charged particles sufficient energy to fly over a potential barrier classically with associated rates which can exceed those from quantum tunneling. For the case of non-relativistic charged particles, the force associated with radiation pressure is proportional to the Thompson cross section. As is shown by Figure 1.2, a charged particle can temporarily receive an extra energy from quantum radiation pressure fluctuations allowing it to fly over the potential barrier. If this barrier potential is

wide enough, the vacuum radiation pressure effect can always dominate over usual quantum tunneling. Indeed, for sufficiently large incident energies and small values of the parameter decay, the barrier penetration rate caused by vacuum radiation pressure fluctuations may be large enough to be observable. Similar results are obtained for the case of polarizable particles.

Chapter 2

Diagonalization of the quadratic bosonic stress tensor

So far, we have studied the probability distribution for quantum stress operators by analyzing the behavior of high moments of these operators. Now we proceed to develop an independent test of the moment-based approach, in which we diagonalize $\overline{S}$ and express the Minkowski vacuum vector in the basis of its eigenstates. Note that the vacuum is not in general an eigenstate of the time averaged quantum stress tensor operator, $\overline{S}$. Using the expression for the vacuum in terms of the new basis allows us to calculate the probability distribution function of obtaining a specific result in a measurement of $\overline{S}$. This approach can yield information about the contribution of various modes and occupation numbers to the probability distribution, in addition to providing a uniquely defined probability distribution.

2.1 Bogoliubov diagonalization

We express a general quadratic operator H as a mode sum involving bosonic creation and annihilation operators for N modes as

$$H = \frac{1}{2}\sum_{ij}^{N}\left(a_i^\dagger D_{1ij} a_j + a_i^\dagger D_{2ij} a_j^\dagger + a_i D_{3ij} a_j + a_i D_{4ij} a_j^\dagger\right), \tag{2.1}$$

where

$$\left[a_i, a_j^\dagger\right] = \delta_{ij}\mathbb{1} \quad \text{and} \quad [a_i, a_j] = \left[a_i^\dagger, a_j^\dagger\right] = 0\,, \tag{2.2}$$

and $\mathbb{1}$ is the identity operator. Here the coefficients of Eq. (2.1) correspond to elements of N-square matrices $\{D_r\}_{r=1}^4$ which form the so-called dynamical matrix

$$\mathcal{D} = \begin{pmatrix} D_1 & D_2 \\ \\ D_3 & D_4 \end{pmatrix}. \tag{2.3}$$

Here we follow an approach developed by Colpa [42] for the diagonalization of $\mathcal{D}$. This approach was previously applied to stress tensor operators by Dawson [43], who was primarily concerned with quantum inequality bounds on expectation values. The diagonalization of the quadratic operator H implies a homogeneous linear transformation (Bogoliubov transformation [44]) to go from the original set of bosonic operators, $(a_i, a_i^\dagger)_{i=1}^N$, to a new one, $(b_i, b_i^\dagger)_{i=1}^N$, in which H takes a diagonal form. For our purposes, we consider the case $D_1 = D_4 = F$ and $D_2 = D_3 = G$ with F and G real and symmetric matrices. Under these conditions, we may normal order the operator H in Eq. (2.1) to obtain

$$:H: = \frac{1}{2}\left(2\mathbf{a}^\dagger F \mathbf{a} + \mathbf{a}^T G \mathbf{a} + \mathbf{a}^\dagger G \mathbf{a}^{\dagger T}\right), \tag{2.4}$$

with

$$\text{with} \quad \mathbf{a} \equiv \begin{pmatrix} a_1 \\ \\ a_2 \\ \\ \vdots \\ \\ a_N \end{pmatrix} \quad \text{and} \quad \mathbf{a}^\dagger \equiv \begin{pmatrix} a_1^\dagger & a_2^\dagger & \cdots & a_N^\dagger \end{pmatrix}, \tag{2.5}$$

and the superscript T denotes a transpose. Here we have combined the first and last terms in Eq. (2.1) using the fact that F is real and symmetric. Note that the operator $\overline{S}$ in Eq. (1.44) takes this form, in the case of infinite N,

where $F = \tilde{A}$ and $G = 2\tilde{B}$. An important observation is that we may use the canonical commutation relations (2.2) to write

$$:H: = \frac{1}{2}\begin{pmatrix}\mathbf{a}^\dagger & \mathbf{a}^T\end{pmatrix}\begin{pmatrix}F & G\\ G & F\end{pmatrix}\begin{pmatrix}\mathbf{a}\\ \mathbf{a}^{\dagger T}\end{pmatrix} - \frac{1}{2}\mathrm{Tr}(F)\mathbb{1}\,. \tag{2.6}$$

Now we apply a Bogoliubov transformation

$$\mathbf{a} = A\mathbf{b} + B\mathbf{b}^{\dagger\,T}, \quad \text{with} \quad \mathbf{b} \equiv \begin{pmatrix} b_1\\ b_2\\ \vdots\\ b_N\end{pmatrix} \quad \text{and} \quad \mathbf{b}^\dagger \equiv \begin{pmatrix} b_1^\dagger & b_2^\dagger & \dots & b_N^\dagger\end{pmatrix}, \tag{2.7}$$

where A and B are real $N \times N$ matrices, and the new set of bosonic operators satisfy the usual commutation relations $[b_i, b_j^\dagger] = \delta_{ij}\mathbb{1}$ and $[b_i, b_j] = [b_i^\dagger, b_j^\dagger] = 0$. Note that the commutation relations for the a and $a^\dagger$ operators and the Bogoliubov transformation, Eq. (2.7), impose conditions upon A and B matrices of the form

$$AA^T - BB^T = I \quad \text{and} \quad AB^T - BA^T = 0\,, \tag{2.8}$$

where I and 0 are the identity and null $N \times N$ matrices, respectively. A consequence of these equations is that $(A - B)(A^T + B^T) = I$, so $A \pm B$ is invertible with inverse $A^T \mp B^T$. Substituting Eq. (2.7) into Eq. (2.6), we obtain

$$:H: = \frac{1}{2}\begin{pmatrix}\mathbf{b}^\dagger & \mathbf{b}^T\end{pmatrix}\begin{pmatrix}A^T & B^T\\ B^T & A^T\end{pmatrix}\begin{pmatrix}F & G\\ G & F\end{pmatrix}\begin{pmatrix}A & B\\ B & A\end{pmatrix}\begin{pmatrix}\mathbf{b}\\ \mathbf{b}^{\dagger T}\end{pmatrix} - \frac{1}{2}\mathrm{Tr}(F)\mathbb{1}\,. \tag{2.9}$$

Now we impose a diagonalization condition

$$\begin{pmatrix}A^T & B^T\\ B^T & A^T\end{pmatrix}\begin{pmatrix}F & G\\ G & F\end{pmatrix}\begin{pmatrix}A & B\\ B & A\end{pmatrix} = \begin{pmatrix}\Lambda & 0\\ 0 & \Lambda\end{pmatrix}, \tag{2.10}$$

in Eq. (2.9), where $\Lambda = \mathrm{diag}(\lambda_1, \ldots, \lambda_N)$. Using the canonical commutation relations for the b_i, we obtain

$$:H: = \sum_{i=1}^{N} \lambda_i b_i^\dagger b_i + C_{\mathrm{shift}} \mathbb{1}\,, \tag{2.11}$$

where

$$C_{\mathrm{shift}} = \frac{1}{2}\mathrm{Tr}(\Lambda - F). \tag{2.12}$$

It is clear that $:H:$ is diagonal in the orthonormal basis formed by vectors

$$|\mathbf{n}\rangle_b = \left(\prod_{i=1}^{N} \frac{(b_i^\dagger)^{n_i}}{\sqrt{n_i!}} \right) |0\rangle_b \tag{2.13}$$

where $\mathbf{n} = (n_1, \ldots, n_N)$ with each n_i a nonnegative occupation number, so that $b_i^\dagger b_i |\mathbf{n}\rangle_b = n_i |\mathbf{n}\rangle_b$ and $|0\rangle_b$ is annihilated by all the b_i. The eigenvalues are easily read off from

$$:H:|\mathbf{n}\rangle_b = (n_i \lambda_i + C_{\mathrm{shift}})|\mathbf{n}\rangle_b\,, \tag{2.14}$$

where the i-index runs from 1 to N, and a sum on repeated indices is understood. If $\lambda_1, \ldots, \lambda_N$ are all positive, then the operator $:H:$ is bounded from below and C_{shift} is the lowest eigenvalue. This gives a quantum inequality bound

$$\langle\psi|:H:|\psi\rangle \geq C_{\mathrm{shift}} \tag{2.15}$$

for all physical normalized states ψ. Note that C_{shift} is both the lowest eigenvalue of the time-averaged stress tensor operator, and the lower bound on its probability distribution, $P(x)$, so that $C_{\mathrm{shift}} = -x_0$.

Let us return to the problem of achieving the diagonalization in practice. Noting that Eq. (2.8) can be written in matrix notation as

$$\begin{pmatrix} A & -B \\ -B & A \end{pmatrix} \begin{pmatrix} A^T & B^T \\ B^T & A^T \end{pmatrix} = \begin{pmatrix} I & 0 \\ 0 & I \end{pmatrix}\,, \tag{2.16}$$

we use the diagonalization condition, Eq. (2.10), to obtain

$$\begin{pmatrix} F & G \\ G & F \end{pmatrix} \begin{pmatrix} A & B \\ B & A \end{pmatrix} = \begin{pmatrix} A & -B \\ -B & A \end{pmatrix} \begin{pmatrix} \Lambda & 0 \\ 0 & \Lambda \end{pmatrix} \tag{2.17}$$

$$= \begin{pmatrix} A\Lambda & -B\Lambda \\ -B\Lambda & A\Lambda \end{pmatrix}, \tag{2.18}$$

which is equivalent to a set of $2N$-equations to be solved for A, B, and Λ, given F and G:

$$(F+G)(A+B) = (A-B)\Lambda\,, \tag{2.19}$$

$$(F-G)(A-B) = (A+B)\Lambda\,. \tag{2.20}$$

A consequence of these equations and $(A \pm B)^{-1} = (A \mp B)^T$ is that

$$(A+B)^T(F+G)(A+B) = \Lambda = (A-B)^T(F-G)(A-B) \tag{2.21}$$

and as we are interested in the case where Λ is positive definite, it follows that a solution is only possible if both $F+G$ and $F-G$ are also positive definite. In this case, the equations can be solved as follows. First, because $F-G$ is positive, we may use the Cholesky decomposition [45] to find a real and invertible matrix K such that $K^\dagger K = F-G$. The matrix $K(F+G)K^\dagger$ is real, symmetric and positive definite and therefore can be brought to diagonal form $U^\dagger K(F+G)K^\dagger U$ where all the diagonal entries are strictly positive and U is a real orthogonal matrix. We then define

$$\Lambda = \sqrt{U^\dagger K(F+G)K^\dagger U} \tag{2.22}$$

It may be verified (see App. A.1) that the solution to (2.19) and (2.20) is

given by Λ together with

$$A = \frac{1}{2}(\Phi + \Psi) \quad \text{and} \quad B = \frac{1}{2}(\Phi - \Psi)\,, \tag{2.23}$$

where

$$\Phi = K^\dagger U \Lambda^{-1/2} \quad \text{and} \quad \Psi = (F+G)\Phi\Lambda^{-1}\,. \tag{2.24}$$

2.2 Probabilities for the single-mode case

Now that we have the real matrices, A and B, we want to express the original vacuum state, $|0\rangle_a$, as a linear combination of the eigenstates of $\overline{S} = :H:$, Eq. (2.4), which are linear combinations of the $|n_i\rangle_b$ in the new b-basis. First, we will develop the simplest case, a single mode, to obtain insight into the general case. The single mode case shows some interesting features which hold for the general case. In this case, A and B become 1×1 matrices, or real numbers. Express

$$|0\rangle_a = \sum_{n=0}^{\infty} C_n |n\rangle_b, \tag{2.25}$$

where C_n are coefficients to be determined. Apply the a-annihilation operator from the left and use the Bogoliubov transformation for the single mode case, Eq. (2.7), according to

$$0 = a|0\rangle_a = \sum_{n=0}^{\infty} C_n (Ab + Bb^\dagger)|n\rangle_b\,, \tag{2.26}$$

$$= C_1 A|0\rangle_b + \sum_{n=0}^{\infty} \left(C_{n+2} A\sqrt{n+2}|n+1\rangle_b + C_n B\sqrt{n+1}|n+1\rangle_b \right)\,. \tag{2.27}$$

Now apply $(|0\rangle_b)^\dagger$ from the left to obtain $C_1 = 0$. Then, Eq. (2.27) becomes

$$\sum_{n=0}^{\infty} \left(C_{n+2} A\sqrt{n+2} + C_n B\sqrt{n+1} \right) |n+1\rangle_b = 0\,. \tag{2.28}$$

As the $|n\rangle_b$ form an orthonormal basis, we deduce

$$C_{n+2} = -A^{-1}B\sqrt{\frac{n+1}{n+2}}C_n\,. \tag{2.29}$$

From this recursive expression and the fact that $C_1 = 0$, we have that all C_n coefficients with odd-n are zero. The a-vacuum is only connected with $|2n\rangle_b$ eigenstates of $\overline{S}$. Let us make explicit this feature of the system and relabel n by $2n$ in Eq. (2.29) and define $\mathcal{M} \equiv A^{-1}B$ to obtain

$$C_{2n+2} = -\mathcal{M}\sqrt{\frac{2n+1}{2(n+1)}}C_{2n}\,. \tag{2.30}$$

It can be proved by induction that the general term in Eq. (2.30) has the form (see App. A.2)

$$C_{2n} = \left(-\frac{\mathcal{M}}{2}\right)^n \frac{\sqrt{(2n)!}}{n!}\mathcal{N} \quad \text{for} \quad n = 0, 1, 2, 3, \dots\,, \tag{2.31}$$

where $\mathcal{N} \equiv C_0$. We apply the normalization condition to obtain $\mathcal{N}$ as

$${}_a\langle 0|0\rangle_a = 1 = \sum_{n',n=0}^{\infty} C^*_{2n'}C_{2n}\ {}_b\langle 2n'|2n\rangle_b = \frac{|\mathcal{N}|^2}{\sqrt{1-\mathcal{M}^2}}\,, \quad \text{with} \quad |\mathcal{M}| < 1. \tag{2.32}$$

Then $|\mathcal{N}| = (1-\mathcal{M}^2)^{1/4}$. Here we have used Eq. (2.25) and the orthonormality property of the a-vacuum. Substituting the expression for $\mathcal{N}$ into Eq. (2.31), we have

$$C_{2n} = \left(-\frac{\mathcal{M}}{2}\right)^n \frac{\sqrt{(2n)!}}{n!}(1-\mathcal{M}^2)^{1/4}\,, \quad \text{for} \quad n = 0, 1, 2, 3, \dots\,. \tag{2.33}$$

As a result, the probability P_{2n} of finding the original a-vacuum state in a specific b-state, $|2n\rangle_b$, and the corresponding eigenvalue of $\overline{S}$, Eq. (2.11), are given by

$$P_{2n} = |{}_b\langle 2n|0\rangle_a|^2 = |C_{2n}|^2\,, \tag{2.34}$$

$$\overline{S}|2n\rangle_b = (2n\lambda + C_{\text{shift}})\,|2n\rangle_b\,, \tag{2.35}$$

where $n = 0, 1, 2, 3 \ldots$. From these equations, we see that the lowest possible outcome in a measurement of $\overline{S}$ is just $C_{\text{shift}} = (\lambda - F)/2$, the a-vacuum state is only connected with $2n$-particle sectors of the b-state, and the probability of finding the a-vacuum state in a specific b-state is concentrated in the lower particle number sectors. Indeed, the asymptotic expression for P_{2n} decreases rapidly with n according to

$$P_{2n} \sim |\mathcal{N}|^2 \frac{\mathcal{M}^{2n}}{\sqrt{\pi n}}, \quad \text{for large } n \text{ and } |\mathcal{M}| < 1. \tag{2.36}$$

These three features of the single mode case hold for the general case that we now proceed to develop in the next section.

2.3 Probabilities for the general case

Express the a-vacuum state as a linear combination of ψ_n, where each ψ_n belongs to the n-particle subspace for b-states, as follows

$$|0\rangle_a = \sum_{n=0}^{\infty} \psi_n \,. \tag{2.37}$$

Apply the a_i-annihilation operator from the left, use the Bogoliubov transformation, Eq. (2.7), and define again $\mathcal{M} \equiv A^{-1}B$ (now $\mathcal{M}$ is a matrix). In detail,

$$b_k^\dagger \left[b_k + \mathcal{M}_{kj} b_j^\dagger \right] |0\rangle_a = b_k^\dagger (A^{-1})_{ki} (A_{ij} b_j + B_{ij} b_j^\dagger) |0\rangle_a = (A^{-1})_{ki} b_k^\dagger a_i |0\rangle_a = 0 \,, \tag{2.38}$$

where a sum on repeated indices is understood. So,

$$0 = \sum_{n=0}^{\infty} \left[b_k^\dagger b_k + b_k^\dagger \mathcal{M}_{kj} b_j^\dagger \right] \psi_n \,, \tag{2.39}$$

$$= \psi_1 + \sum_{n=2}^{\infty} \left[n\psi_n + (\mathbf{b}^\dagger \mathcal{M} \mathbf{b}^{\dagger T}) \psi_{n-2} \right] , \tag{2.40}$$

where we have used $b_k^\dagger b_k \psi_n = n\psi_n$ in the last line. The expression inside the bracket in Eq. (2.40) consists of n-particle terms with $n \geq 2$, thus we can only

have a solution with $\psi_1 = 0$. That means that

$$\psi_n = -\frac{1}{n}\left(\mathbf{b}^\dagger \mathcal{M} \mathbf{b}^{\dagger T}\right)\psi_{n-2} \quad \text{for n } \geq 2 \tag{2.41}$$

and $\psi_1 = \psi_3 = \cdots = \psi_{2n+1} = 0$. We can rewrite Eq. (2.41) by relabeling n by $2n$ and expressing ψ_{2n} in terms of ψ_0 as

$$\psi_{2n} = \frac{(-1)^n}{2^n n!}\left(\mathbf{b}^\dagger \mathcal{M} \mathbf{b}^{\dagger T}\right)^n \psi_0 \,. \tag{2.42}$$

Now, define $\psi_0 = \mathcal{N}|0\rangle_b$ to obtain

$$|0\rangle_a = \sum_{n=0}^{\infty} \psi_{2n} = \mathcal{N}\sum_{n=0}^{\infty}\left(-\frac{1}{2}\right)^n \frac{1}{n!}\left(\mathbf{b}^\dagger M \mathbf{b}^{\dagger T}\right)^n |0\rangle_b \,, \tag{2.43}$$

$$= \mathcal{N} e^{-\frac{1}{2}\mathbf{b}^\dagger \mathcal{M} \mathbf{b}^{\dagger T}} |0\rangle_b \,, \tag{2.44}$$

where $\mathcal{N}$ is a normalization constant to be determined. Now, we diagonalize $\mathcal{M}$ such that $\mathcal{M} = R^T \Xi S$ with R a real and orthogonal matrix and $\Xi = \mathrm{diag}(\mu_i)$. Set $c_i = R_{ij} b_j$ and $c_i^\dagger = R_{ij} b_j^\dagger$. They satisfy the bosonic commutation relations, because

$$[c_i, c_k] = [R_{ij} b_j, R_{kl} b_l] = R_{ij} R_{kl} [b_j, b_l] = 0 \,, \tag{2.45}$$

$$[c_i, c_k^\dagger] = R_{ij} R_{kl} [b_j, b_l^\dagger] = (R R^T)_{ik} = \delta_{ik} \,. \tag{2.46}$$

Here we have used the commutation relation of b-operators and the orthogonality of R. Now note that we can rewrite the exponent in Eq. (2.44) using

$$\mathbf{b}^\dagger \mathcal{M} \mathbf{b}^{\dagger T} = b_i^\dagger \left(R^T \Xi R\right)_{ij} b_j^\dagger = \mu_l R_{li} R_{lj} b_i^\dagger b_j^\dagger = \mu_l c_l^\dagger c_l^\dagger \,, \tag{2.47}$$

where a sum on repeated indices is understood. Then the a-vacuum expressed in terms of the b-states, Eq. (2.44), becomes

$$|0\rangle_a = \mathcal{N} e^{-\frac{1}{2}\sum_i \mu_i c_i^\dagger c_i^\dagger} |0\rangle_b \,. \tag{2.48}$$

The normalization constant $\mathcal{N}$ is calculated using the a-vacuum normalization and the definition for $c_i^\dagger$'s. For a single mode we have

$$
\begin{aligned}
{}_a\langle 0|0\rangle_a = 1 &= |\mathcal{N}|^2 \left\| \sum_{n=0}^{\infty} \frac{-(\mu/2)^n}{n!} (c^\dagger)^{2n} |0\rangle_b \right\|^2 , && (2.49)\\
&= |\mathcal{N}|^2 \left\| \sum_{n=0}^{\infty} \frac{(-\mu/2)^n}{n!} \sqrt{(2n)!} |2n\rangle_b \right\|^2 , && (2.50)\\
&= |\mathcal{N}|^2 (1-\mu^2)^{-1/2} , \quad \text{with} \quad |\mu| < 1 . && (2.51)
\end{aligned}
$$

Then $|\mathcal{N}| = (1-\mu^2)^{1/4}$. As expected, we have recovered the result of the previous subsection, Eq. (2.32), noting that for the single-mode case $\mu = \mathcal{M}$. For the multimode situation, we have (see App. A.3)

$$
|\mathcal{N}| = \prod_i (1-\mu_i^2)^{1/4} . \tag{2.52}
$$

The probability $P_{\{n_i\}}$ of finding the a-vacuum state in a specific b-state, $|\{n_k\}\rangle_b$, which now depends upon N-modes, can be obtained from Taylor expanding the exponential in Eq. (2.44) according to

$$
\begin{aligned}
P_{\{n_k\}} = |{}_b\langle \{n_k\}|0\rangle_a|^2 &= \left| {}_b\langle \{n_k\}| \mathcal{N} e^{-\frac{1}{2}\mathbf{b}^\dagger \mathcal{M} \mathbf{b}^{\dagger T}} |0\rangle_b \right|^2 , && (2.53)\\
&= \left| {}_b\langle \{n_k\}| \mathcal{N} \left(1 - \frac{1}{2} \sum_{i,j=1}^{N} b_i^\dagger \mathcal{M}_{ij} b_j^\dagger + \dots \right) |0\rangle_b \right|^2 , && (2.54)\\
&= \left| {}_b\langle \{n_k\}| \mathcal{N} \left(|0\rangle_b - \frac{1}{\sqrt{2}} \sum_{i=1}^{N} \mathcal{M}_{ii} |2_i\rangle_b - \sum_{i<j}^{N} \mathcal{M}_{ij} |1_i 1_j\rangle_b + \dots \right) \right|^2 . && (2.55)
\end{aligned}
$$

From this expression, we can determine, for example, the probability of finding the system in the b-vacuum state, $P_{\{0\}}$, or in some configuration in the two-particle sector such as $P_{\{2_i\}}$ or $P_{\{1_i 1_j\}}$. These probabilities and the corresponding outcomes associated with a measurement of $\overline{S} = :H:$, Eq. (2.11), are

specifically given by

$$P_{\{0\}} = |\mathcal{N}|^2\,, \quad \text{and} \quad \overline{S}|0\rangle_b = C_{\text{shift}}|0\rangle_b\,, \tag{2.56}$$

$$P_{\{2_i\}} = (1/2)|\mathcal{N}|^2|M_{ii}|^2\,, \quad \text{and} \quad \overline{S}|2_i\rangle_b = (2\lambda_i + C_{\text{shift}})\,|2_i\rangle_b\,, \tag{2.57}$$

$$P_{\{1_i 1_j\}} = |\mathcal{N}|^2|M_{ij}|^2\,, \quad \text{and} \quad \overline{S}|1_i 1_j\rangle_b = (\lambda_i + \lambda_j + C_{\text{shift}})\,|1_i 1_j\rangle_b\,. \tag{2.58}$$

Here $i < j$ in Eq. (2.58) and i, j run from 1 to N for Eqs. (2.56 - 2.58). Now, we can re-express the normalization constant, $\mathcal{N}$, to obtain information about the total probability for each particle sector. We take Eq. (2.52) and write the product as a determinant of the $\mathcal{M}$ matrix as

$$|\mathcal{N}|^2 = \prod_i (1-\mu_i^2)^{1/2} = \sqrt{\det(1-\mathcal{M}^2)} = e^{\frac{1}{2}\text{Tr}[\log(1-\mathcal{M}^2)]}\,, \tag{2.59}$$

where we have used the formula $\det(W) = \exp\{\text{Tr}[\log(W)]\}$ for a given matrix, W (see App. A.4). Expressing the log-function as an infinite power series, and Taylor expanding the exponential, we can recognize the contribution for each particle sector as follows

$$1 = |\mathcal{N}|^2 e^{-\frac{1}{2}\text{Tr}[\log(1-\mathcal{M}^2)]} = |\mathcal{N}|^2 e^{\frac{1}{2}\sum_{n=1}^{\infty}\frac{\text{Tr}(\mathcal{M}^{2n})}{n}}\,, \tag{2.60}$$

$$\begin{aligned} &= |\mathcal{N}|^2 + |\mathcal{N}|^2\left[\frac{1}{2}\text{Tr}(\mathcal{M}^2)\right] + |\mathcal{N}|^2\left[\frac{1}{4}\text{Tr}(\mathcal{M}^4) + \frac{1}{8}\text{Tr}^2(\mathcal{M}^2)\right] \\ &\quad + |\mathcal{N}|^2\left[\frac{1}{8}\text{Tr}(\mathcal{M}^2)\text{Tr}(\mathcal{M}^4) + \frac{1}{48}\text{Tr}^3(\mathcal{M}^2) + \frac{1}{6}\text{Tr}(\mathcal{M}^6)\right] + \mathcal{O}(\mathcal{M}^8)\,. \end{aligned} \tag{2.61}$$

Then, the contributions to the total probability of the b-vacuum and the two-particle sector, for instance, are $|\mathcal{N}|^2$ and $(1/2)|\mathcal{N}|^2\text{Tr}(\mathcal{M}^2)$, respectively. Each $2n$-particle sector contributes with terms having $2n$-factors of $\mathcal{M}$.

Chapter 3

Massless scalar field in Minkowski spacetime

3.1 Square of the time derivative of the field

We consider a minimally coupled massless scalar field, $\phi(t, \mathbf{r})$, in a four-dimensional Minkowski spacetime in spherical coordinates (t, r, θ, φ), with the origin of the spherical polar coordinates placed at the fixed spatial point at which $:\dot{\phi}^2:$ will be evaluated. We choose this particular operator to facilitate comparison of our results with those of Ref. [11], which focused on this operator for simplicity. The equation of motion is given by the usual wave equation

$$\Box\, \phi(t, \mathbf{r}) = 0\,. \tag{3.1}$$

Solutions of this equation take the form [37]

$$u_{\omega lm} = \frac{g_{\omega l}(r)}{\sqrt{2\omega}} Y_{lm}(\theta, \varphi) e^{-i\omega t}\,, \tag{3.2}$$

where

$$g_{\omega l}(r) = \omega \sqrt{\frac{2}{R}} j_l(\omega r)\,, \tag{3.3}$$

and

$$1 = \int_0^R r^2 g_{\omega l}^2(r) dr \,. \tag{3.4}$$

Here $j_l(\omega r)$ and $Y_{lm}(\theta, \varphi)$ are the spherical Bessel functions and the usual spherical harmonics, respectively. The normalization, Eq. (3.4), is carried out in a sphere of radius R. We set vanishing boundary conditions on the surface of the sphere by requiring

$$\phi(r)|_{r=R} = 0 \,, \tag{3.5}$$

which implies

$$\omega = \frac{z_{nl}}{R} \,, \quad n = 1, 2, \ldots \,. \tag{3.6}$$

Here z_{nl} is the nth zero of the spherical Bessel function, j_l.

We expand the quantized field in terms of creation and annihilation operators, $a_{\omega lm}$ and $a^\dagger_{\omega lm}$, as

$$\phi(t, \mathbf{r}) = \sum_{l=0}^{\infty} \sum_{m=-l}^{l} \sum_{\omega} \left(a_{\omega lm} u_{\omega lm} + a^\dagger_{\omega lm} u^*_{\omega lm} \right) \,, \tag{3.7}$$

where a sum on ω is abbreviated notation for the sum on $n = 1, 2, \ldots$ with ω taking the values (3.6) for the angular momentum sector l in question.

We want to calculate the time average of the normal-ordered quadratic operator $:\dot{\phi}^2:$ at fixed spatial point $r = 0$ with sampling function $f(t)$, as in Eq. (1.13). Since all $l \neq 0$ spherical Bessel functions vanish at $r = 0$, we only have to consider the case $l = m = 0$. Then, using $j_0(\omega r) = [\sin(\omega r)]/(\omega r)$ and $Y_{00} = 1/\sqrt{4\pi}$ in Eq. (3.2), we have

$$u_{\omega 00}(t, r) = \frac{\sin(\omega r)}{r} \frac{e^{-i\omega t}}{\sqrt{4\pi\omega R}} \,, \tag{3.8}$$

which, in the limit when $r \to 0$, becomes

$$u_{\omega 00}(t, 0) = \sqrt{\frac{\omega}{4\pi R}} e^{-i\omega t} \,. \tag{3.9}$$

Note that from the boundary conditions on the sphere, Eq.(3.6), we have that $z_{n0} = n\pi$, so

$$\omega = \frac{n\pi}{R} \,, \quad n = 1, 2, \ldots \,. \tag{3.10}$$

Making these simplifications in Eq. (3.7), taking the time derivative, and forming the Wick square, we obtain

$$:\dot{\phi}^2:(t,\mathbf{0}) = \sum_{\omega}\sum_{\omega'} \frac{(\omega\omega')^{3/2}}{4\pi R}\left(a^\dagger_\omega a_{\omega'} e^{i(\omega-\omega')t} - a_\omega a_{\omega'} e^{-i(\omega+\omega')t} + H.c.\right), \quad (3.11)$$

where $a_\omega \equiv a_{\omega 00}$, the sums run over the range given in Eq. (3.10), and $H.c.$ means hermitian conjugate. Convergence here should be understood in a distributional sense, so that when we now let $S = \dot{\phi}^2$ in Eq. (1.13), we find

$$\overline{S} = \sum_{\omega}\sum_{\omega'} \frac{(\omega\omega')^{3/2}}{4\pi R}\left[a^\dagger_\omega a_{\omega'} \hat{f}(\omega'-\omega) - a_\omega a_{\omega'}\hat{f}(\omega+\omega') + H.c.\right], \quad (3.12)$$

where $\hat{f}$ is the Fourier transform of the sampling function $f(t)$.

We consider two different classes of sampling functions: the Lorentzian function, $f_L(t)$, whose Fourier transform is given by Eq. (1.16) ($\alpha = 1$) and compactly supported functions, $f_{\rm cs}(t)$, whose Fourier transform has an asymptotic form when $\omega\tau \gg 1$ given by Eq. (1.38) ($\alpha \in (0,1)$). For this last case, we use a set of smooth, even, and nonnegative functions $f_{\rm cs}(t) : \mathbb{R} \to [0,\infty)$ with compact support in $[-2\delta, 2\delta]$ and with Fourier transform given by (see Secs. IIA and IIB of Ref. [11])

$$\hat{f}_{\rm cs}(\omega) = \frac{\hat{H}^2(\omega) + \frac{1}{2}\left[\hat{H}^2\left(\omega+\frac{\pi}{2\delta}\right) + \hat{H}^2\left(\omega-\frac{\pi}{2\delta}\right)\right]}{\hat{H}^2(0) + \hat{H}^2\left(\frac{\pi}{2\delta}\right)}. \quad (3.13)$$

Here $\hat{H}(\omega)$ is the Fourier transform of $H(t) = \varphi(t+\delta)\varphi(\delta-t)$, with $\varphi(t)$ being the inverse Laplace transform of $\tilde{\varphi}(p) = e^{-(p\tau)^\alpha}$. The Fourier transform $\hat{f}_{\rm cs}(\omega)$ is analytic, even, nonnegative and is normalized to one, $\hat{f}_{\rm cs}(0) = 1$. When $\omega\tau \gg 1$, $\hat{f}_{\rm cs}(\omega)$ has the asymptotic form given by Eq. (1.38) with

$$\gamma = \frac{4\varphi^2(2\delta)}{\hat{H}^2(0) + \hat{H}^2(\frac{\pi}{2\delta})}, \quad (3.14)$$

$$\beta = 2\cos\left(\frac{\pi\alpha}{2}\right). \quad (3.15)$$

Figure 3.1 plots the compactly supported function $f_{\rm cs}(t)$ and its Fourier transform $\hat{f}_{\rm cs}(\omega)$ for the cases of $\alpha = 1/2$, $\alpha = 0.6$, and $\alpha = 0.7$. The plots for the

$\alpha = 1/2$ case agree with those in Figs. 4 and 5 in Ref. [11], where the function and its Fourier transform were called $L(t)$ and $\hat{L}(\omega)$, respectively. It should be noted that τ is not the duration of the sampling period, which is 4δ, but rather sets the decay rate of the high frequency components in the sampling function and corresponds to a characteristic timescale of the switch-on and switch-off parts of $f_{\rm cs}(t)$. However it can serve as a proxy for the overall sampling time, within a set of functions related to f by scaling. Using τ in this way also facilitates comparison with the Lorentzian function, for which the total sampling duration is infinite.

We define dimensionless variables $x_1 = \overline{S}(\tau^2)^2$ and $x_2 = \overline{S}(4\pi\tau^2)^2$ for the compactly supported functions and the Lorentzian function, respectively. (The difference in the numerical factors is to facilitate comparison with the results of Refs. [10] and [11], which used slightly different conventions.) Using the expression for ω, Eq. (3.10), these variables become

$$x_1 = \frac{1}{2}\sum_{r,s=1}^{\infty} \frac{\tau_0^4}{2\pi^2}(rs)^{3/2}\left[a_r^\dagger a_s \hat{f}_{\rm cs}(|r-s|\tau_0) - a_r a_s \hat{f}_{\rm cs}((r+s)\tau_0) + H.c.\right], \tag{3.16}$$

and

$$x_2 = \frac{1}{2}\sum_{r,s=1}^{\infty} 8\tau_0^4(rs)^{3/2}\left(a_r^\dagger a_s e^{-|r-s|\tau_0} - a_r a_s e^{-(r+s)\tau_0} + H.c.\right), \tag{3.17}$$

where we have defined

$$\tau_0 \equiv \pi\tau/R\,. \tag{3.18}$$

Note that the expressions for x_1 and x_2 have the form of Eq. (2.4). Thus, the matrices F and G for the case of a compactly supported function are

$$F_{rs} = \frac{\tau_0^4}{2\pi^2}(rs)^{3/2}\hat{f}_{\rm cs}(|r-s|\tau_0) \quad \text{and} \quad G_{rs} = -\frac{\tau_0^4}{2\pi^2}(rs)^{3/2}\hat{f}_{\rm cs}((r+s)\tau_0)\,. \tag{3.19}$$

Similarly, those for the case of a Lorentzian sampling function are

$$F_{rs} = 8\tau_0^4(rs)^{3/2}e^{-|r-s|\tau_0} \quad \text{and} \quad G_{rs} = -8\tau_0^4(rs)^{3/2}e^{-(r+s)\tau_0}\,. \tag{3.20}$$

The F and G matrices are all that we need to calculate, for a given number of modes, the probability distribution and the cumulative probability distribution

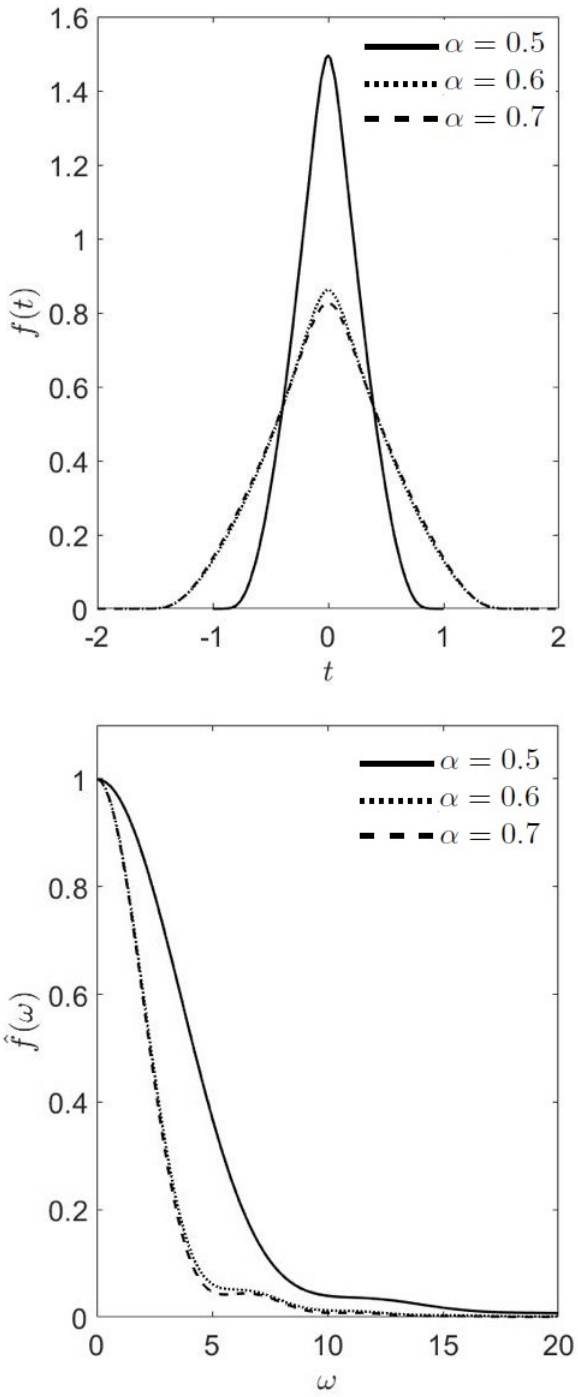

Figure 3.1: Plots for the compactly supported function $f_{\text{cs}}(t)$ (upper figure) and its Fourier transform $\hat{f}_{\text{cs}}(\omega)$ (lower figure), for the cases of $\alpha = 0.5$ (solid line), $\alpha = 0.6$ (dotted line), and $\alpha = 0.7$ (dashed line). The values for δ used for each of these cases are, respectively, $0.5, 0.9$, and 1.0, and units in which $\tau = 1$ are used.

associated with a measurement of x_1 or x_2.

3.2 Numerical results for the tail of $P(x)$

Here we explain the general features of the numerical calculation that we carry out to calculate the probability, $P(x)$, and cumulative probability distribution function, $P_<(x) = 1 - P_>(x)$, for the two cases mentioned above. Here x denotes either x_1 or x_2, defined in Eqs. (3.16) and (3.17). For a given number of modes, we calculate all possible outcomes in a measurement of x up to and including the 6-particle sector, except for the following outcomes which have been omitted:

$$\lambda_i + \lambda_j + \lambda_k + \lambda_l + \lambda_m + \lambda_n + C_{\text{shift}} \,, \tag{3.21}$$

$$2\lambda_i + \lambda_j + \lambda_k + \lambda_l + \lambda_m + C_{\text{shift}} \,. \tag{3.22}$$

Recall that the λ_i are the one-particle eigenvalues which appear in Eq. 2.11. Here it is understood all indices are different in these expressions. These outcomes were not included due to the large number of operations that they would entail. For example, the outcome with six different eigenvalues, Eq. (3.21), would involve about 10^9 operations for the case of 100 modes. All probabilities and outcomes included in the calculation are listed explicitly in Appendix B. We build the cumulative distribution $P_<(x)$ by adding the probabilities of outcomes, $P_{\{n_i\}}$, from Eq. (2.55), which are sorted from the lowest to the largest value of x.

The number of modes and the value for τ_0 are crucial in determining the quality of the $P_<(x)$-curve. Recall that we have standing waves, Eq. (3.2), inside a sphere of radius R, which is related to τ and τ_0 by Eq. (3.18), and that the sampling timescale τ is defined for the Lorentzian function in Eq. (1.16), and for the compactly supported functions in Eqs. (1.38), (3.13), (3.14) and (3.15). For a fixed characteristic timescale, τ, the radius of the sphere is inversely proportional to the dimensionless variable τ_0. For a given number of modes, if the size of the sphere is too large, there will not be enough data in the tail ($x \gg 1$) of the $P_<(x)$-curve to perform a reliable fit. By contrast, if the size of the sphere is too small, the $P_<(x)$-curve will not be smooth, showing a step-like behavior. For the compactly supported functions, we also have to

determine values for δ, which defines the support of the sampling function $f_{\rm cs}(t)$, i.e., the duration of the sampling. We choose these values to be slightly larger than the first maximum of the corresponding $\varphi(t)$. The larger the decay parameter, the larger this maximum and the chosen value for δ. Results are given in Table 3.1, working in units where $\tau = 1$. Then the sphere radius $R = \tau_0/\pi$ gives values 1.14, 0.64 and 0.64 for $\alpha = 0.5, 0.6, 0.7$, respectively, for the values of τ_0 considered. Note that for $\alpha = 0.5$ we have $R > 2\delta$, which means that the total sampling time is less than the time taken for light to travel to the boundary and back. Accordingly, the numerics ought to give a good approximation to sampling in Minkowski space; this is an instance of local covariance, which has a number of applications to quantum inequalities [46]. By contrast, in the other two remaining cases we have $R < 2\delta$, so the sampling process can be sensitive to the presence of the bounding sphere. The slighlty increased values of δ used for $\alpha = 0.6, 0.7$ provides us the best numerical stability.

We build $P_<(x)$-curves for compactly supported functions whose Fourier transform is given by Eq. (3.13) with three different values of the decay parameter, $\alpha = (0.5, 0.6, 0.7)$, and the Lorentzian function. Table 3.1 summarizes the main characteristic of these curves which are shown by Figs. 3.2 and 3.3 for the range $450 \lesssim x \lesssim 10000$. All curves are smooth, show the presence of large vacuum fluctuations ($x \gg 1$), and have sufficient amount of data to carry out the subsequent fit procedure. Recall that the original a-vacuum state is expressed in terms of a linear combination of b-states which are eigenstates of x. As expected, the most likely b-state is the b-vacuum state and the $P_<(x)$-curves are bounded below by the value $C_{\rm shift} = -x_0 < 0$. The loss of probability for each case is given by $[1 - P_<(x_{max})]$, where x_{max} is the maximum value obtained in a measurement of x for a given number of modes and size of the sphere. All analyzed cases show a small loss of probability of the order of 10^{-5} or less. This small loss of probability indicates that the outcomes which have been included provide a reasonable approximation for $P_<(x)$.

Our calculated values of the lower bound $C_{\rm shift}$ can be compared with results from other approaches. In the case of the Lorentzian function, our calculated value $C_{\rm shift} = -0.0593338$, is of the order of the predicted value from the analysis using high moments, $x_0 = -0.0236$ in Eq. (1.32) and well within the (non-optimal) theoretical bound $C_{\rm shift} \geq -27/128 = -0.211$ given by the

Table 3.1: Numerical results for the parameters of the $P_<(x)$-curves illustrated in Figs. 3.2 and 3.3, for the case of compactly supported functions with different values of α and for the Lorentzian function. Units in which $\tau = 1$ have been adopted. Here values of $P_<(x)$ for different particle sectors are calculated adding all probabilities for all possible outcomes for the given sector as is indicated in Table A.1. Since x_{max} is the maximum value obtained in a measurement of x for a given number of modes and size of the sphere, the expression $[1 - P_<(x_{max})]$ gives us the loss of probability.

	$\boldsymbol{P_<(x_1)\ \ \alpha = 0.5}$	$\boldsymbol{P_<(x_1)\ \ \alpha = 0.6}$
Modes	120	120
Points	$\mathcal{O}(10^9)$	$\mathcal{O}(10^9)$
$\boldsymbol{\delta}$	0.5	0.9
$\boldsymbol{\gamma}$	2.9324	1.0433
$\boldsymbol{\beta}$	1.4142	1.1756
$\boldsymbol{f\,(0)}$	1.4990	0.8616
$\boldsymbol{\tau_0}$	3.5725	2.0
$\boldsymbol{x_{max}}$	$\mathcal{O}(10^8)$	$\mathcal{O}(10^7)$
$\mathbf{C}_{\text{shift}}$	$-7.81613 \cdot 10^{-2}$	$-1.48420 \cdot 10^{-2}$
Vacuum	$9.88503 \cdot 10^{-1}$	$9.72841 \cdot 10^{-1}$
$\mathbf{2^{nd}}$**sector**	$1.13068 \cdot 10^{-2}$	$2.61008 \cdot 10^{-2}$
$\mathbf{4^{nd}}$**sector**	$1.86704 \cdot 10^{-4}$	$1.01218 \cdot 10^{-3}$
$\mathbf{6^{nd}}$**sector**	$3.44828 \cdot 10^{-6}$	$4.38949 \cdot 10^{-5}$
$\boldsymbol{[1 - P_<(x_{max})]}$	$6.83316 \cdot 10^{-8}$	$2.09890 \cdot 10^{-6}$
	$\boldsymbol{P_<(x_1)\ \ \alpha = 0.7}$	$\boldsymbol{P_<(x_2)}$ **Lorentzian**
Modes	120	140
Points	$\mathcal{O}(10^9)$	$\mathcal{O}(10^9)$
$\boldsymbol{\delta}$	1.0	–
$\boldsymbol{\gamma}$	0.5235	1
$\boldsymbol{\beta}$	0.9080	1
$\boldsymbol{f\,(0)}$	0.8274	0.6366
$\boldsymbol{\tau_0}$	2.0	0.2
$\boldsymbol{x_{max}}$	$\mathcal{O}(10^7)$	$\mathcal{O}(10^6)$
$\mathbf{C}_{\text{shift}}$	$-1.37113 \cdot 10^{-2}$	$-5.93338 \cdot 10^{-2}$
Vacuum	$9.71898 \cdot 10^{-1}$	$9.70277 \cdot 10^{-1}$
$\mathbf{2^{nd}}$**sector**	$2.69537 \cdot 10^{-2}$	$2.87007 \cdot 10^{-2}$
$\mathbf{4^{nd}}$**sector**	$1.09604 \cdot 10^{-3}$	$9.48946 \cdot 10^{-4}$
$\mathbf{6^{nd}}$**sector**	$4.97286 \cdot 10^{-5}$	$2.97518 \cdot 10^{-5}$
$\boldsymbol{[1 - P_<(x_{max})]}$	$2.49384 \cdot 10^{-6}$	$4.37397 \cdot 10^{-5}$

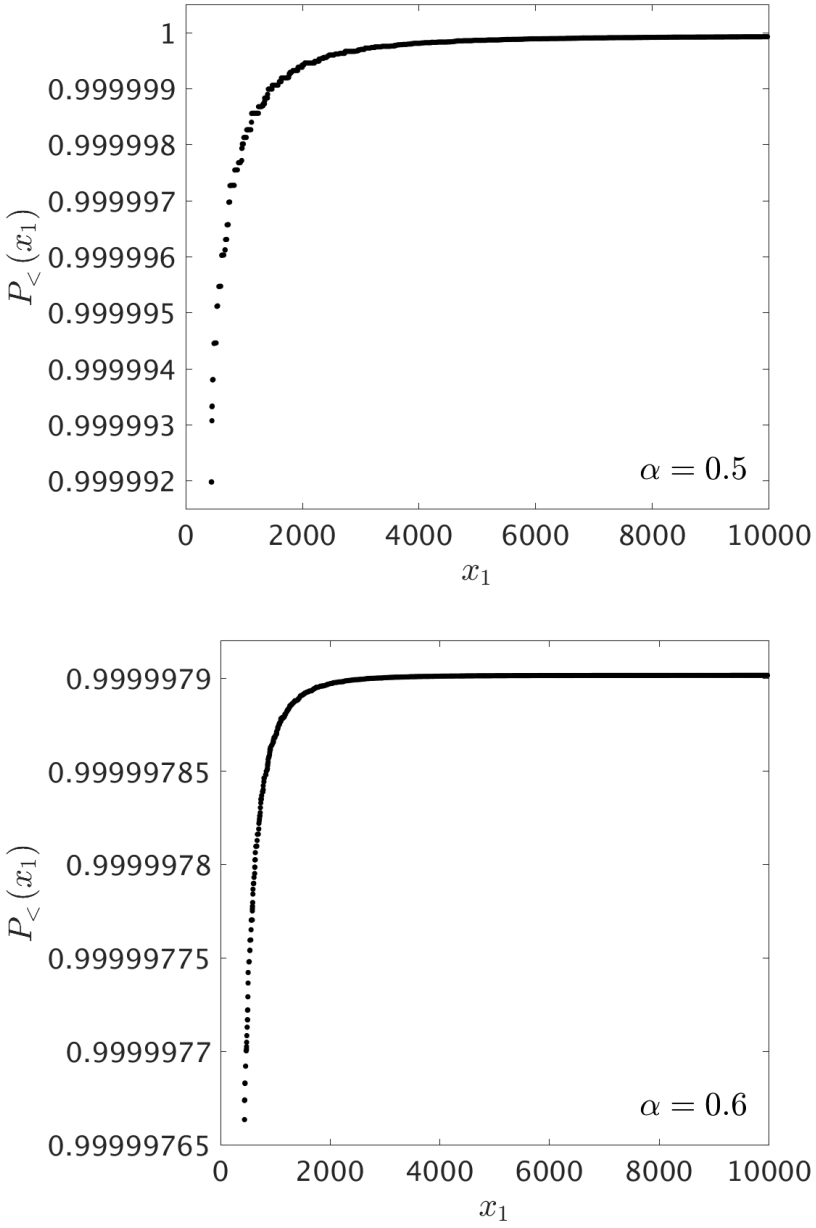

Figure 3.2: $P_<(x)$-curves for the case of compactly supported functions with decay parameters of $\alpha = 0.5$ (upper figure) and $\alpha = 0.6$ (lower figure) for the range $450 \lesssim x \lesssim 10000$. Additional information is shown in detail in Table 3.1.

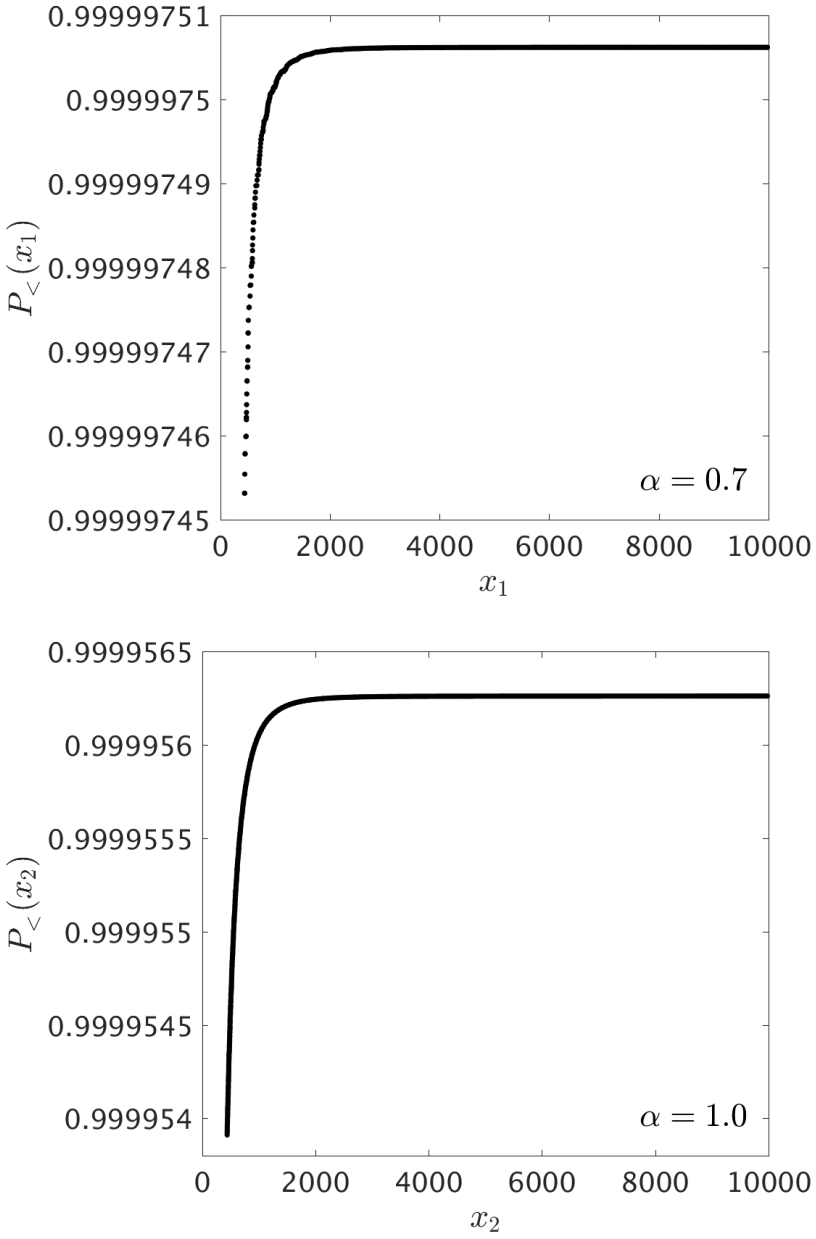

Figure 3.3: $P_<(x)$-curves for the case of compactly supported functions with decay parameter of $\alpha = 0.7$ (upper figure) and the Lorentzian function (lower figure) for the range $450 \lesssim x \lesssim 10000$. Additional information is shown in detail in Table 3.1.

method of [38]. For a general compactly supported test function f, the theoretical bound is

$$C_{\text{shift}} \geq -\frac{\tau^4}{16\pi^2}\int_{-\infty}^{\infty}\left\{[f(t)^{1/2}]''\right\}^2 dt \tag{3.23}$$

which can be obtained by setting $p = \sqrt{\omega}$ in Eq. (3.11) of [38]. For the case $\alpha = 0.5$, the integral on the right-hand side of Eq. (3.23) can be evaluated numerically and yields the bound $C_{\text{shift}} \geq -0.3592$. Our calculated value $C_{\text{shift}} = -0.0781613$ is therefore consistent with the theoretical bound and indicates that the latter bound is weaker than the sharpest possible bound by a factor of approximately 4.6. This result is broadly in line with Dawson's computations [43], where a ratio of about 3 was found. Note that Dawson used a toroidal spatial geometry rather than a ball and a squared Lorentzian sampling function of infinite duration, so one would not expect an exact match with our results.

Since we want to test the predicted behavior of the cumulative probability distribution for large fluctuations in vacuum, we focus on the tail of each $P_<(x)$-curve and propose a trial function inspired by Eq. (1.52). Specifically,

$$P_<(x;\hat{\theta}) = p_1 - \frac{c_0 a^{-(1+b)/c}}{c}\Gamma\left(\frac{1+b}{c}, ax^c\right). \tag{3.24}$$

Here $\hat{\theta} = (p_1, a, b, c, c_0)$ are the five free parameters to be determined through the usual process of best-fitting. We fit the numerical data to this trial function. Producing a $P_<(x)$-curve implies propagating errors from the successive sum of the $P_{\{n_i\}}$, defined in Eq. (2.55), but errors coming from the diagonalization procedure are mostly dominated by the error in $|N|^2$, from the vacuum sector. Constructing the tail of each $P_<(x)$-curve entails dealing with 10^6 data points. To make the fitting-procedure possible in a reasonable time, we bin the data as follows. Let N be the total number of data points. We split this set in several subsets N_i, where $N = \sum_{i=1}^{j} N_i$ and j is the total number of subsets. Consider one subset of values of x and the associated values of $P_<(x)$, $N_i = \{(x_1, P_<(x_1)), (x_2, P_<(x_2)), \ldots, (x_{N_i}, P_<(x_{N_i}))\}$. Next replace it by the averaged values $\overline{N}_i = (\bar{x}_i, \overline{P}_<(\bar{x}_i))$, where $\bar{x}_i = \sum_{k=1}^{N_i} x_k/N_i$ and $\overline{P}_<(\bar{x}_i) = \sum_{k=1}^{N_i} P_<(x_k)/N_i$. The size of the subset is taken to depend on the steepness of the $P_<(x)$-curve. The steeper this curve, the smaller is N_i. This procedure ensures that the best fit to the set of averaged values represents a good fit of the original curve. The 10^6 data points are typically divided into about 10^3 bins. The values of N_i, the number of points per bin, range from

about 10^2 at the smaller values of x to about 10^4 at the larger values.

The fitting procedure is based on the least-squares method to find the specific set of values of parameters which minimize the error variance. We name this specific set as $\theta^* = (p_1^*, a^*, b^*, c^*, c_0^*)$. The estimation of the error variance, s^2, is given by

$$s^2 = \frac{1}{(j-5)} \sum_{i=1}^{j} \frac{\left[\overline{P}_<(\bar{x}_i) - P_<(\bar{x}_i; \hat{\theta})\right]^2}{(N/N_i)}, \tag{3.25}$$

where $(j-5)$ is the number of degrees of freedom,$\overline{P}_<(\bar{x}_i)$ is the ith value of the averaged $\overline{P}_<(\bar{x})$-curve, $P_<(\bar{x}_i; \hat{\theta})$ is the ith value of the fitting-curve. Note that we are weighting each ith value of the square of the residuals, $[\ \overline{P}_<(\bar{x}) - P_<(\bar{x}_i; \hat{\theta})\ ]^2$, by the ratio (N/N_i). This gives a greater weight to the larger subsets. We have also assumed that the error in the values associated with the j different subsets is the same. This allows us to directly sum the squares of the residuals over the various subsets. If the errors of the different subsets are different, then weight factors for each subset would be needed.

Table 3.2 summarizes the statistical information obtained by the best-fitting procedure for each case which includes the estimate value for parameters and their respective standard errors (only from statistical sources). Figure 3.4 shows the $\overline{P}_<(\bar{x})$-curves with their respective best fits to the trial function, Eq. (3.24). In the case of the Lorentzian function, the $\overline{P}_<(\bar{x})$-curve and its respective fit are indistinguishable on the scale shown. Figure 3.4 shows that the diagonalization procedure is able to reproduce smooth tails for all the cases considered, which are well fitted by the trial function given by an incomplete gamma function, Eq. (3.24). The variance of the fits are small in comparison to the variation of the $\overline{P}_<(\bar{x})$-curves. For example, for the case of the compactly supported function with $\alpha = 0.7$, we have $s^2 \sim \mathcal{O}(10^{-22})$ but the change of the $\overline{P}_<(\bar{x})$-curve over the range plotted in Fig. 3.4 is the order of 10^{-9}.

All values of parameters obtained through the best-fitting procedure agree reasonably well with the predicted ones from the high moments approach (see Table 3.2 for the case of the Lorentzian function and Eqs. (1.54) and (1.55) for the case of compactly supported functions), except for those for the c_0 parameter. The deviations of the fitted values for this parameter from to the predicted values, which are of $\mathcal{O}(1)$ or less, are probably caused by the use a finite number of modes and finite size of the sphere. The most important parameter to be evaluated is c, due to it is related to the rate of decrease of the probability distribution for large fluctuations, Eq. (1.1). Recall that $c = \alpha/3$,

Table 3.2: Parameters obtained from the best fit of Eq. (3.24) for compactly supported functions with different values of α, and for the Lorentzian function.

	$\boldsymbol{\alpha = 0.5}$ $\boldsymbol{(s^2 \sim 10^{-18})}$		
	Estimate	Standard Error	Theoretical [11]
$\boldsymbol{p_1^*}$	1	$9.86890 \cdot 10^{-10}$	1
$\boldsymbol{a^*}$	3.21574	0.26916	3.19965
$\boldsymbol{b^*}$	-0.64913	$6.74595 \cdot 10^{-2}$	-1
$\boldsymbol{c^*}$	0.17368	$6.21754 \cdot 10^{-3}$	0.16667
$\boldsymbol{c_0^*}$	$1.24953 \cdot 10^{-2}$	$6.17359 \cdot 10^{-3}$	$4.84678 \cdot 10^{-2}$
	$\boldsymbol{\alpha = 0.6}$ $\boldsymbol{(s^2 \sim 10^{-21})}$		
	Estimate	Standard Error	Theoretical [11]
$\boldsymbol{p_1^*}$	1	$3.82057 \cdot 10^{-12}$	1
$\boldsymbol{a^*}$	2.86707	$3.09190 \cdot 10^{-3}$	3.04545
$\boldsymbol{b^*}$	-1.29164	$1.94800 \cdot 10^{-3}$	-1.13333
$\boldsymbol{c^*}$	0.198625	$1.74722 \cdot 10^{-4}$	0.2
$\boldsymbol{c_0^*}$	$5.52294 \cdot 10^{-2}$	$8.36918 \cdot 10^{-4}$	$1.57857 \cdot 10^{-2}$
	$\boldsymbol{\alpha = 0.7}$ $\boldsymbol{(s^2 \sim 10^{-22})}$		
	Estimate	Standard Error	Theoretical [11]
$\boldsymbol{p_1^*}$	1	$6.87424 \cdot 10^{-13}$	1
$\boldsymbol{a^*}$	2.74969	$1.18528 \cdot 10^{-3}$	2.47920
$\boldsymbol{b^*}$	-1.17210	$5.71700 \cdot 10^{-4}$	-1.26667
$\boldsymbol{c^*}$	0.228107	$1.15423 \cdot 10^{-4}$	0.23333
$\boldsymbol{c_0^*}$	$3.05954 \cdot 10^{-2}$	$3.22838 \cdot 10^{-4}$	$5.44308 \cdot 10^{-3}$
	Lorentzian $\boldsymbol{(s^2 \sim 10^{-17})}$		
	Estimate	Standard Error	Theoretical [10]
$\boldsymbol{p_1^*}$	0.99996	$5.44678 \cdot 10^{-11}$	1
$\boldsymbol{a^*}$	1.04998	$1.19509 \cdot 10^{-2}$	0.667749
$\boldsymbol{b^*}$	-1.14578	$9.33892 \cdot 10^{-3}$	-2
$\boldsymbol{c^*}$	0.315336	$1.07643 \cdot 10^{-3}$	0.333333
$\boldsymbol{c_0^*}$	$2.08459 \cdot 10^{-2}$	$8.84006 \cdot 10^{-4}$	0.477696

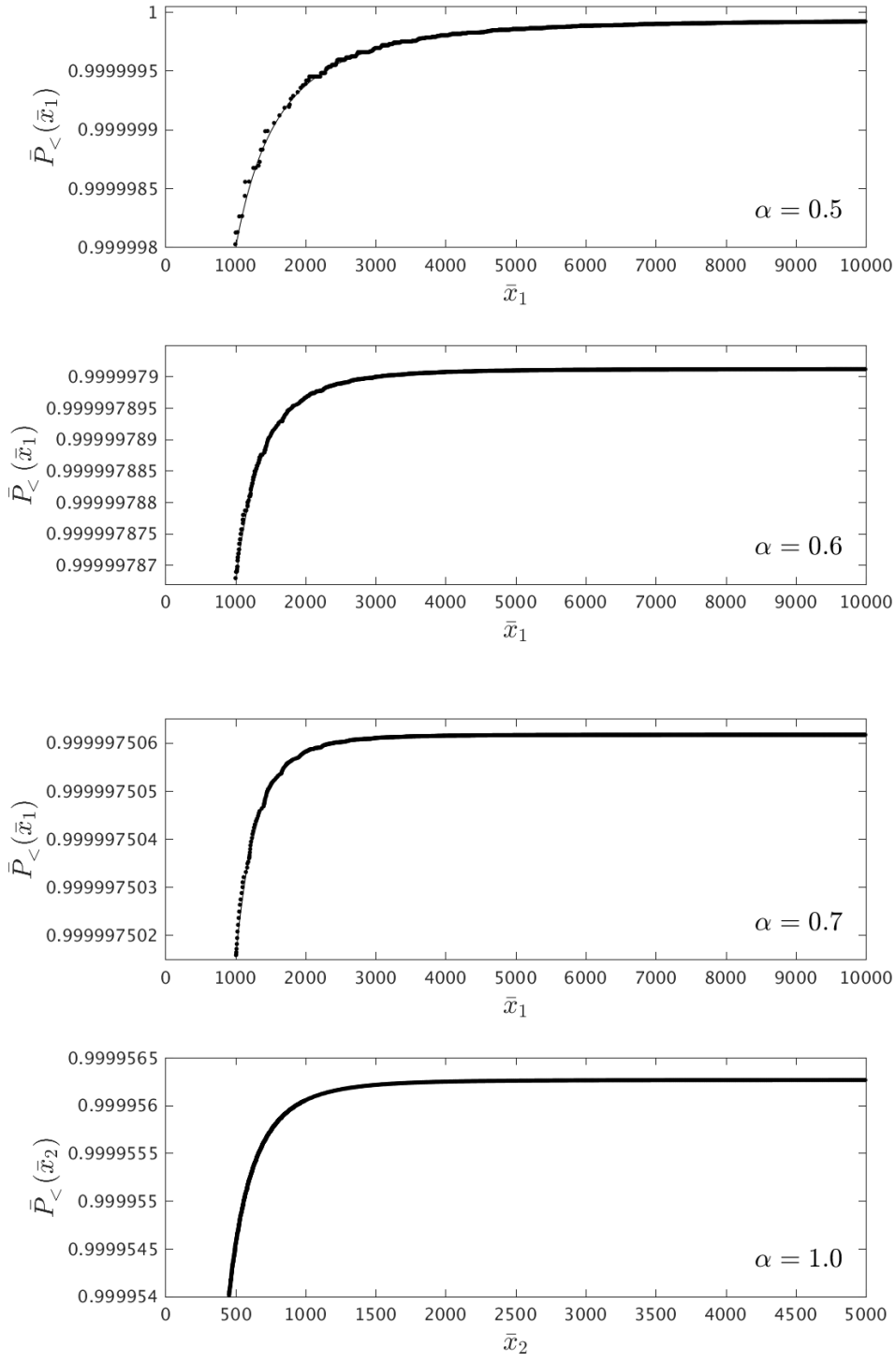

Figure 3.4: Best fitting using Eq. (3.24) to reproduce the $\overline{P}_<(\bar{x})$-curve for the cases of compactly supported functions with different decay parameters (range of $1000 \lesssim x \lesssim 10000$) and for the Lorentzian function (range of $400 \lesssim x \lesssim 5000$). In each case, the dots and the line correspond to the $\overline{P}_<(\bar{x})$-curve and its fit, respectively. For the case of the Lorentzian function, dots and line are indistinguishable on the scale shown.

where $\alpha \in (0,1)$ is the decay parameter for the family of compactly supported functions with Fourier transform given by Eq. (3.13). For the case of a Lorentzian function we have $c = 1/3$. The values of the c parameter obtained for each case agree very well with the predicted ones, with a percentage error less than 6%. For instance, for the case of a compactly supported function with $\alpha = 0.6$, the percentage error is about 0.69%. In complete agreement with previous results based on the high moments analysis (see Secs. 1.2.4 and 1.2.5), our results confirm the fact that averaging over a finite time interval compactly supported functions results in a probability distribution which falls more slowly than for the case of the Lorentzian function, and both fall more slowly than exponentially.

Chapter 4

Summary and Discussion

Large vacuum fluctuations of quantum stress tensor operators can have a variety of physical effects such as production of gravity waves in inflationary models [4], fluctuations of the light propagation speed in nonlinear materials [5, 6], and enhancing barrier penetration of charged or polarizable particles [7, 8]. These quantum fluctuations can be studied through the analysis of the probability distribution for the time or spacetime averaged operator in Minkowski spacetime. The asymptotic behavior of the probability distribution can be inferred by studying the moments of the normal ordered operator. The study of several normal-ordered quadratic operators time averaged with a Lorentzian function [10] or compactly supported functions [11] predict an asymptotic form of the probability distribution for large vacuum fluctuations x given by $P(x) \sim c_0 x^b e^{-ax^c}$, Eq. (1.1), where x is a dimensionless measure of the quadratic operator. This form leads to an asymptotic form for the cumulative probability distribution given by an incomplete gamma function, Eq. (1.52). Here c_0, a, b, and c are constants which depend on the sampling function used to take the time average. The c-parameter is the most important one, and defines the rate of decrease of the tail of the probability distribution. For the family of compactly supported functions with asymptotic Fourier transforms given by Eq. (1.38), where $0 < \alpha < 1$, we have $c = \alpha/3$. For the case of a Lorentzian function, Eq. (1.16), we have $\alpha = 1$ and $c = 1/3$. The smaller α, the smaller the rate of decrease of the tail and greater the probability of large fluctuations. The value of α is related to the rate of switch-on and switch-off of compactly supported functions.

In the present thesis, we have developed a method which is independent of the moments approach for the study of the probability distribution for quantum vacuum fluctuations of a time averaged quantum stress tensor operator, $\overline{S}$, in Eq. (1.13). Since the vacuum state is not usually an eigenstate of $\overline{S}$, we diagonalize this operator through a change of basis. Expressing the vacuum state in terms of the new basis in which $\overline{S}$ is diagonal, we are able to calculate the probability distribution, $P(x)$ and the cumulative probability distribution function, $P_<(x)$ for obtaining a specific result in a measurement of $\overline{S}$. Specifically, we work with the time averaged quadratic operator $\overline{S} = \int_{-\infty}^{\infty} :\dot{\phi}^2(t,0): f(t)dt$, where ϕ is a massless minimally coupled scalar field and $f(t)$ is the sampling function . We use a dimensionless variable $x \propto \overline{S}\tau^4$, where τ is a characteristic timescale of the sampling function. Numerical results for both Lorentzian and compactly supported functions show that the probability distribution of vacuum quantum fluctuations is bounded below at $x = -x_0 < 0$, and that the tail of the cumulative probability distribution varies as an incomplete gamma function in agreement with the previous studies shown in Secs. 1.2.4 and 1.2.5. We apply a best-fit procedure through a least-squares method to the tail of the $P_<(x)$-curves in order to determine values for parameters in Eq. (3.24). The results for $p_1, a, b, \text{and } c$ parameters show good agreement with the predictions of the high moments approach. (See Table 3.2.) The diagonalization procedure is able to reproduce with great accuracy the rate of decrease of the tail of the cumulative probability distribution. We reproduce the relation $c = \alpha/3$ for $\alpha = (0.5, 0.6, 0.7, 1)$, where $\alpha = 1$ corresponds to the case of the Lorentzian function, with percentage errors less than 6% compared to the theoretical values predicted by the high moments approach (see Table 3.2 for the case of the Lorentzian function and Eqs. 1.54 and 1.55 for the case of compactly supported functions). Our results confirm that averaging over a finite time interval, with compactly supported functions, results in a probability distribution which falls more slowly than for the case of Lorentzian averaging, and both fall more slowly than exponentially.

Recall that we have quantized the scalar field in a sphere with finite radius R, so the probability distribution which we calculate could differ from that of empty Minkowski spacetime. As was noted in Sect. 3.2, there should be no difference for the $\alpha = 1/2$ case, as the duration of the sampling is less than the light travel time to the boundary and back. In the other cases, there could in principle be an effect of the boundary. However, this is likely only to alter the lower frequency modes, which are not expected to give a large contribution to the tail of the distribution.

The diagonalization method is free of the ambiguity potentially present in the high moments approach, and leads to a unique result for the probability distribution. It also has the potential to determine the entire distribution, including its lower bound, which is also the optimum quantum inequality bound on expectation values of the averaged operators. In addition, it can provide information about the particle content of the eigenstates of the averaged stress tensor which are associated with the large fluctuations.

Future directions based on this thesis include the following possible research lines: (1) to analyze the effect of considering a spatial (or spatial and temporal) average of stress tensor operators, (2) to study different fields in a free or interacting theory, such as a Dirac field including a Yukawa interaction or a scalar field including a four point interaction, (3) to explore effects of large stress fluctuations on curved spacetime such as a Schwarzschild background in the framework of black hole physics, and (4) to apply the theoretical frame developed in this thesis to other areas of interest such as condensed matter systems.

Including a spatial average of stress tensor operators or quadratic operators needs to be explored. For example, taking a spatial average of the time average of the normal-ordered quadratic operator $:\dot{\phi}^2:$ analyzed in Chap. 3 requires considering a more general solution for the modes u_{wlm}, Eq. (3.7), with nonzero values of l and m. The vanishing boundary conditions on the sphere surface lead to Eq. (3.6), $\omega = (z_{nl}/R)$, where z_{nl} is the nth zero of the spherical Bessel function and R is the sphere radius. Note that the simple relation $\omega = (n\pi/R)$ for $n = 1, 2, 3, ...$ is no longer valid for solutions with nonzero angular momentum. If we consider a spatial sampling function which only radial dependence, the expression for $\overline{S}$, Eq. (3.12), would include a radial integration of the product between the spatial sampling function and two spherical Bessel functions.

Exploring large stress fluctuations considering a massive scalar field plus a four point interaction, could potentially have interesting implications. That is because this case is related to axion dark matter in the small field approximation. Recently there has been much interest in studying the spatial distribution of light scalar dark matter throughout the universe. If the local gravitational interactions between the scalar modes are rapid enough, the field can re-organize into a Bose-Einstein condensate (BEC) of short range order; a type of localized clump, as was explained in Ref. [47]. A detailed exploration of these axion clumps was perfomed in Refs. [48], [49], and [50], a series of papers written by me during my graduate studies in collaboration with Prof. Mark

P. Hertzberg. We studied in Ref. [48] spherically symmetric configurations (BEC ground states) of the axion-gravity-self-interacting system and found two branches of solutions which exist primarily in the non-relativistic regime. One branch is stable and the other is unstable: clumps which are spatially large are stable, while clumps which are spatially small are unstable and may collapse. In both cases, there is a maximum number of particles which can be in a clump. The stable branch is mainly ruled by gravity and could comprise a significant component of dark matter in the galaxy. We extended this work in Ref. [49] by considering higher angular momentum eigenstates that break the spherical symmetry and generalized previous results from spherical configurations. In particular, while there is still a maximum number of particles (and hence a maximum mass), its value increases with angular momentum. We considered in Ref. [50] the axion clump resonance of photons, since the axion clump oscillates coherently. We found that for spherically symmetric clumps the resonance is absent for conventional values of the QCD axion to photon coupling, but it could happen for non-standard QCD axions or generic scalar dark matter with repulsive interactions. We extended these results to non-spherically symmetric clumps finding that even QCD axion clumps can show resonant decay when the angular momentum is large enough. Including quantum fluctuations in the analysis of axion clumps would give us a more accurate picture about their stability and astrophysical properties.

Appendix A

Some calculations

A.1 Bogoliubov transformation

Here we derive Eqs. (2.23) and (2.24), which are the solutions of the Eqs. (2.19) and (2.20) in terms of the positive definite diagonal matrix Λ and the real matrices A and B, for given real and symmetric matrices F and G.

The expression $\Lambda = \sqrt{U^T K(F+G)K^T U}$ entails $U\Lambda^2 U^{-1} = K(F+G)K^T$, where $K^\dagger = K^T$ and $U^{-1} = U^T$. Then, with $\Phi = K^T U \Lambda^{-1/2}$ and $\Psi = (F+G)\Phi\Lambda^{-1}$, we have

$$(F+G)\Phi = \Psi\Lambda \tag{A.1}$$

by definition and also $K\Psi = K(F+G)\Phi\Lambda^{-1} = U\Lambda^{1/2}$. Then

$$(F-G)\Psi = K^T K\Psi = K^T U\Lambda^{1/2} = \Phi\Lambda\,. \tag{A.2}$$

Using the definitions of A and B from Eq. (2.23), Equations (A.1) and (A.2) lead to Eqs. (2.19) and (2.20), respectively, according to

$$(F+G)(A+B) = (F+G)\Phi = \Psi\Lambda = (A-B)\Lambda\,, \tag{A.3}$$

$$(F-G)(A-B) = (F-G)\Psi = \Phi\Lambda = (A+B)\Lambda\,. \tag{A.4}$$

Finally, using $\Phi\Psi^T = K^T U \Lambda^{-1/2}(K^{-1}U\Lambda^{1/2})^T = I$ and hence $\Psi\Phi^T = I$, we have

$$AA^T - BB^T = \frac{1}{2}(\Phi\Psi^T + \Psi\Phi^T) = I\,, \tag{A.5}$$

$$AB^T - BA^T = \frac{1}{2}(\Psi\Phi^T - \Phi\Psi^T) = \frac{1}{2}(I - I) = 0\,, \tag{A.6}$$

where I and 0 correspond to the identity and null matrices, respectively. These equations are the conditions that A and B have to satisfy in order to define a Bogoliubov transformation, Eq. (2.8).

A.2 Inductive proof of the general term C_{2n}

From Eq. (2.30), we consider the following recurrence equation and initial condition:

$$C_{2n} = \begin{cases} \mathcal{N} & \text{if } n = 0 \\ -\mathcal{M}\sqrt{\frac{2n-1}{2n}}C_{2n-2} & \text{for } n = 1, 2, 3, \ldots \end{cases} \tag{A.7}$$

We will prove using induction that the general term is given by Eq. (2.31) following the next three steps:

(i) The base case is trivial as we have defined $C_0 = \mathcal{N}$ and the general term for $n = 0$ gives us

$$C_0 = \left(-\frac{\mathcal{M}}{2}\right)^0 \frac{\sqrt{(2\cdot 0)!}}{0!}\mathcal{N} = \mathcal{N}\,. \tag{A.8}$$

(ii) Assume that the general term is true for $n-1$, $C_{2(n-1)}$.
(iii) We prove that the general term is true for n, C_{2n}. From the recurrence, we have

$$C_{2n} = -\mathcal{M}\sqrt{\frac{2n-1}{2n}}C_{2n-2}\,. \tag{A.9}$$

Using the inductive hypothesis, replace C_{2n-2} into Eq. (A.9) and work out as

follows

$$C_{2n} = -\mathcal{M}\sqrt{\frac{2n-1}{2n}}\left(-\frac{\mathcal{M}}{2}\right)^{n-1}\frac{\sqrt{(2n-2)!}}{(n-1)!}\mathcal{N}\,, \tag{A.10}$$

$$= \left(-\frac{\mathcal{M}}{2}\right)^{n}\sqrt{\frac{2n(2n-1)(2n-2)!}{n^2(n-1)!(n-1)!}}\mathcal{N}\,, \tag{A.11}$$

$$= \left(-\frac{\mathcal{M}}{2}\right)^{n}\frac{\sqrt{(2n)!}}{n!}\mathcal{N}\,. \tag{A.12}$$

A.3 Normalization for the multimode case

Using Eqs. (2.48) and (2.51), we have for the multimode situation

$${}_a\langle 0|0\rangle_a = 1 = \left\|\mathcal{N}e^{-\frac{1}{2}\sum_i \mu_i c_i^\dagger c_i^\dagger}|0\rangle_b\right\|^2\,, \tag{A.13}$$

$$= |\mathcal{N}|^2\left\|\prod_i e^{-\frac{1}{2}\mu_i c_i^\dagger c_i^\dagger}|0\rangle_b\right\|^2\,, \tag{A.14}$$

$$= |\mathcal{N}|^2\prod_i \left\|(1-\mu_i^2)^{-1/2}\right\|^2,\ \text{with } |\mu_i|<1\,, \tag{A.15}$$

$$= |\mathcal{N}|^2\prod_i (1-\mu_i^2)^{-1/4}\,. \tag{A.16}$$

Solving for $\mathcal{N}$, we obtain the normalization constant for the multimode case, Eq. (2.52).

A.4 Determinant and trace of a matrix

Here we prove the formula $\det(W) = \exp\{\mathrm{Tr}[\log(W)]\}$ for a given matrix W. Let P be the orthogonal matrix which diagonalizes W so that $W_o = P^{-1}WP$ is diagonal. Since $\det(W_o) = \mathrm{diag}(w_i)$, where w_i are the eigenvalues

of W, we have

$$\log(W_o) = \mathrm{diag}[\log(w_i)]\,, \tag{A.17}$$

$$\mathrm{Tr}[\log(W_o)] = \sum_i \log(w_i)\,, \tag{A.18}$$

$$e^{\mathrm{Tr}[\log(W_o)]} = e^{\sum_i \log(w_i)} = \prod_i w_i = \det(W_o) = \det(W)\,. \tag{A.19}$$

Here we have taken the trace of Eq. (A.17) to obtain Eq. (A.18) and used $\det(P^{-1}WP) = \det(P^{-1})\det(W)\det(P) = \det^{-1}(P)\det(W)\det(P)$ to obtain the right most equality of Eq. (A.19). Now, expand in Taylor series the logarithm function of W as

$$\log(W) = -\sum_{n=1}^{\infty} \frac{(\mathbb{1} - W)^n}{n} = -\sum_{n=1}^{\infty} \frac{(\mathbb{1} - PW_oP^{-1})^n}{n}\,, \tag{A.20}$$

and apply the trace to the whole equation to obtain

$$\mathrm{Tr}[\log(W)] = -\sum_{n=1}^{\infty} \frac{\mathrm{Tr}\left[(\mathbb{1} - PW_oP^{-1})^n\right]}{n}\,, \tag{A.21}$$

$$= -\sum_{n=1}^{\infty} \frac{\sum_{k=0}^{n} \binom{n}{k} \mathrm{Tr}\left[(-PW_oP^{-1})^k\right]}{n}\,, \tag{A.22}$$

$$= -\sum_{n=1}^{\infty} \frac{\sum_{k=0}^{n} \binom{n}{k} \mathrm{Tr}\left[(P(-W_o)^kP^{-1})\right]}{n}\,, \tag{A.23}$$

$$= -\mathrm{Tr}\left[\sum_{n=1}^{\infty} \frac{(\mathbb{1} - W_o)^n}{n}\right] = \mathrm{Tr}[\log(W_o)]\,. \tag{A.24}$$

Here $\mathbb{1}$ is the identity operator. Note that we have used the binomial identity in Eq. (A.22) and the invariance of the trace under cyclic permutations in Eq. (A.23). Replacing Eq. (A.21) into Eq. (A.19), we obtain the formula which relates the determinant of a given matrix W to its trace as

$$\det(W) = \exp\{\mathrm{Tr}[\log(W)]\}\,. \tag{A.25}$$

A.5 Probabilities and outcomes

We listed below probabilities of finding specific outcomes in a measurement of a time averaged normal ordered quadratic operator. We have only considered up to the 6-particle sector taking out the outcomes given by Eqs. (3.21) and (3.22). It is understood that the coefficients of the $\mathcal{M}$ matrix, which appear in Table A.1, come from the diagonalization procedure explained in Sec. 2.1.

Table A.1: Probabilities and outcomes of a time averaged normal ordered quadratic operator.

Probability	**Outcome**
$\lvert\mathcal{N}\rvert^2$	C_{shift}
$\lvert\mathcal{N}\rvert^2\lvert\mathcal{M}_{ij}\rvert^2$	$\lambda_i+\lambda_j+C_{\text{shift}}$ $^{(a)}$
$\frac{1}{2}\lvert\mathcal{N}\rvert^2\lvert\mathcal{M}_{ii}\rvert^2$	$2\lambda_i+C_{\text{shift}}$
$\frac{3}{8}\lvert\mathcal{N}\rvert^2\lvert M_{ii}\rvert^4$	$4\lambda_i+C_{\text{shift}}$
$\lvert\mathcal{N}\rvert^2\lvert\mathcal{M}_{ij}^2+\frac{1}{2}\mathcal{M}_{ii}\mathcal{M}_{jj}\rvert^2$	$2\lambda_i+2\lambda_j+C_{\text{shift}}$ $^{(a)}$
$\frac{1}{2}\lvert\mathcal{N}\rvert^2\lvert\mathcal{M}_{ii}\mathcal{M}_{jk}+2\mathcal{M}_{ij}\mathcal{M}_{ik}\rvert^2$	$2\lambda_i+\lambda_j+\lambda_k+C_{\text{shift}}$ $^{(b)}$
$\frac{3}{2}\lvert\mathcal{N}\rvert^2\lvert\mathcal{M}_{ii}\rvert^2\lvert\mathcal{M}_{ij}\rvert^2$	$3\lambda_i+\lambda_j+C_{\text{shift}}$
$\lvert\mathcal{N}\rvert^2\lvert\mathcal{M}_{il}\mathcal{M}_{jk}+\mathcal{M}_{ik}\mathcal{M}_{jl}+\mathcal{M}_{ij}\mathcal{M}_{kl}\rvert^2$	$\lambda_i+\lambda_j+\lambda_k+\lambda_l+C_{\text{shift}}$ $^{(c)}$
$\frac{5}{16}\lvert\mathcal{N}\rvert^2\lvert\mathcal{M}_{ii}\rvert^6$	$6\lambda_i+C_{\text{shift}}$
$\frac{15}{8}\lvert\mathcal{N}\rvert^2\lvert M_{ii}\rvert^4\lvert\mathcal{M}_{ij}\rvert^2$	$5\lambda_i+\lambda_j+C_{\text{shift}}$
$\frac{3}{16}\lvert\mathcal{N}\rvert^2\lvert 4\mathcal{M}_{ii}\mathcal{M}_{ij}^2+\mathcal{M}_{ii}^2\mathcal{M}_{jj}\rvert^2$	$4\lambda_i+2\lambda_j+C_{\text{shift}}$
$\frac{1}{4}\lvert\mathcal{N}\rvert^2\lvert 2\mathcal{M}_{ij}^3+3\mathcal{M}_{ii}\mathcal{M}_{ij}\mathcal{M}_{jj}\rvert^2$	$3\lambda_i+3\lambda_j+C_{\text{shift}}$ $^{(a)}$
$\frac{1}{8}\lvert\mathcal{N}\rvert^2\lvert 2\mathcal{M}_{ik}^2\mathcal{M}_{jj}+8\mathcal{M}_{ij}\mathcal{M}_{ik}\mathcal{M}_{jk}+$ $2\mathcal{M}_{ii}\mathcal{M}_{jk}^2+2\mathcal{M}_{ij}^2\mathcal{M}_{kk}+\mathcal{M}_{ii}\mathcal{M}_{jj}\mathcal{M}_{kk}\rvert^2$	$2\lambda_i+2\lambda_j+2\lambda_k+C_{\text{shift}}$ $^{(d)}$
$\frac{3}{8}\lvert\mathcal{N}\rvert^2\lvert\mathcal{M}_{ii}^2\mathcal{M}_{jk}+4\mathcal{M}_{ii}\mathcal{M}_{ij}\mathcal{M}_{ik}\rvert^2$	$4\lambda_i+\lambda_j+\lambda_k+C_{\text{shift}}$ $^{(b)}$
$\frac{1}{4}\lvert\mathcal{N}\rvert^2\lvert 2\mathcal{M}_{ik}\mathcal{M}_{il}\mathcal{M}_{jj}+$ $4\mathcal{M}_{ij}\mathcal{M}_{il}\mathcal{M}_{jk}+4\mathcal{M}_{ij}\mathcal{M}_{ik}\mathcal{M}_{jl}+$ $2\mathcal{M}_{ii}\mathcal{M}_{jk}\mathcal{M}_{jl}+2\mathcal{M}_{ij}^2\mathcal{M}_{kl}+\mathcal{M}_{ii}\mathcal{M}_{jj}\mathcal{M}_{kl}\rvert^2$	$2\lambda_i+2\lambda_j+\lambda_k+\lambda_l+C_{\text{shift}}$ $^{(e)}$
$\frac{3}{4}\lvert\mathcal{N}\rvert^2\lvert 2\mathcal{M}_{ij}^2\mathcal{M}_{ik}+$ $\mathcal{M}_{ii}\mathcal{M}_{ik}\mathcal{M}_{jj}+2\mathcal{M}_{ii}\mathcal{M}_{ij}\mathcal{M}_{jk}\rvert^2$	$3\lambda_i+2\lambda_j+\lambda_k+C_{\text{shift}}$
$\frac{3}{2}\lvert\mathcal{N}\rvert^2\lvert 2\mathcal{M}_{ij}\mathcal{M}_{ik}\mathcal{M}_{il}+\mathcal{M}_{ii}\mathcal{M}_{il}\mathcal{M}_{jk}+$ $\mathcal{M}_{ii}\mathcal{M}_{ik}\mathcal{M}_{jl}+\mathcal{M}_{ii}\mathcal{M}_{ij}\mathcal{M}_{kl}\rvert^2$	$3\lambda_i+\lambda_j+\lambda_k+\lambda_l+C_{\text{shift}}$ $^{(f)}$

Here we have $^{(a)}(i<j)$, $^{(b)}(j<k)$, $^{(c)}(i<j<k<l)$, $^{(d)}(i<j<k)$, $^{(e)}(i<j)\cap(k<l)$, $^{(f)}(j<k<l)$, and the $\mathcal{M}$ matrix is defined in Sec. 2.3.

Bibliography

[1] G. T. Horowitz and R. M. Wald, "Dynamics of Einstein's Equation Modified by a Higher Order Derivative Term," Phys. Rev. D **17**, 414 (1978).

[2] E. D. Schiappacasse and L. H. Ford, "Graviton Creation by Small Scale Factor Oscillations in an Expanding Universe," Phys. Rev. D **94**, no. 8, 084030 (2016).

[3] L. Parker and D. Toms, *Quantum Field Theory in Curved Spacetime*, (Cambridge University Press, 2009), Chap. 4.

[4] C. H. Wu, J. T. Hsiang, L. H. Ford and K. W. Ng, "Gravity Waves from Quantum Stress Tensor Fluctuations in Inflation," Phys. Rev. D **84**, 103515 (2011).

[5] C. H. G. Bessa, V. A. De Lorenci, L. H. Ford and N. F. Svaiter, "Vacuum Lightcone Fluctuations in a Dielectric," Annals Phys. **361**, 293 (2015).

[6] C. H. G. Bessa, V. A. De Lorenci, L. H. Ford and C. C. H. Ribeiro, "Model for lightcone fluctuations due to stress tensor fluctuations," Phys. Rev. D **93**, no. 6, 064067 (2016).

[7] H. Huang and L. H. Ford, "Quantum Electric Field Fluctuations and Potential Scattering," Phys. Rev. D **91**, no. 12, 125005 (2015).

[8] H. Huang and L. H. Ford, "Vacuum Radiation Pressure Fluctuations and Barrier Penetration," Phys. Rev. D **96**, no. 1, 016003 (2017).

[9] C. J. Fewster, L. H. Ford and T. A. Roman, "Probability distributions of smeared quantum stress tensors," Phys. Rev. D **81**, 121901 (2010).

[10] C. J. Fewster, L. H. Ford and T. A. Roman, "Probability distributions for quantum stress tensors in four dimensions," Phys. Rev. D **85**, 125038 (2012).

[11] C. J. Fewster and L. H. Ford, "Probability Distributions for Quantum Stress Tensors Measured in a Finite Time Interval," Phys. Rev. D **92**, no. 10, 105008 (2015).

[12] B. Simon, "The classical moment problem as a self-adjoint finite difference operator," Adv. Math. **137**, 82 (1998).

[13] E. D. Schiappacasse, C. J. Fewster and L. H. Ford, "Vacuum quantum stress tensor fluctuations: A diagonalization approach" Phys. Rev. D **97**, 025013 (2018).

[14] N. D. Birrell and P. C. W. Davies, *Quantum Fields in Curved Space*, (Cambridge University Press, 1982), Chap. 6.

[15] S. W. Hawking, "Particle creation by black holes," Commun. Math. Phys. **43**, 199 (1975).

[16] L. Parker, Quantized fields and particle creation in expanding Universes. I, Phys. Rev. **183**, 1057 (1969); Quantized fields and particle creation in expanding Universes. II, Phys. Rev. D **3**, 346 (1971).

[17] L. H. Ford, "Gravitational particle creation and inflation," Phys. Rev. **D** 35, 2955 (1987).

[18] V. Mukhanov and G. Chibisov, "Quantum fluctuations and a nonsingular universe," JETP Lett. **33**, 532 (1981); A. Guth and S-Y Pi, "Fluctuations in the New Inflationary Universe," Phys. Rev. Lett. **49**, 1110 (1982); J. M. Bardeen, P. J. Steinhardt and M. S. Turner, "Spontaneous creation of almost scale-free density perturbations in an inflationary universe," Phys. Rev. D **28**, 679 (1983).

[19] See, for example, R. Rangarajan, "Inflation after Planck and BICEP2," arXiv:1506.07433 [astro-ph.CO] (2014).

[20] L. H. Ford, "Spacetime in Semiclassical Gravity," arXiv:gr-qc/0504096, (2005).

[21] C. I. Kuo and L. H. Ford, "Semiclassical Gravity Theory and Quantum Fluctuations," Phys. Rev. D **47**, 4510 (1993).

[22] L. H. Ford, "Gravitons and Lightcone Fluctuations," Phys. Rev. D **51**, 1962 (1995).

[23] L. H. Ford, "Gravitons and Lightcone Fluctuations II: Correlations Functions," Phys. Rev. D **54**, 2640 (1996).

[24] L. H. Ford and N. F. Svaiter, Phys. Rev. D **56**, 2226 (1997).

[25] R.D. Sorkin, in Proceedings of the Conference on Heat Kernel Techniques and Quantum Gravity, Canada, 1994, edited by S.A. Fulling (University of Texas Press, 1995), pp. 387-407 [arXiv:gr-qc/9508002]; R.D. Sorkin, in Proceedings of the First Australasian Conference on General Relativity and Gravitation, Australia, 1996, edited by David Wiltshire (University of Adelaide, 1996), pp. 163-174 [arXiv:gr-qc/9701056].

[26] A. Casher, F. Englert, N. Itzhaki, and R. Parentani, Nucl.Phys. B **484**, 419 (1997).

[27] J. Borgman and L. H. Ford, "The Effects of Stress Tensor Fluctuations upon Focusing," Phys. Rev. D **70**, 064032 (2004).

[28] L. H. Ford, S. P. Miao, K. W. Ng, R. P. Woodard and C. H. Wu, "Quantum Stress Tensor Fluctuations of a Conformal Field and Inflationary Cosmology," Phys. Rev. D **82**, 043501 (2010).

[29] C. H. Wu, K. W. Ng, W. Lee, D. S. Lee and Y. Y. Charng, "Quantum Noise and Large-Scale Cosmic Microwave Background Anisotropy," JACP **0702**, 006 (2007).

[30] L. H. Ford, A. D. Helfer and T. A. Roman, "Spatially Averaged Quantum Inequalities Do Not Exist in Four-Dimensional Spacetime," Phys. Rev. D **66**, 124012 (2002).

[31] H. Epstein, V. Glaser and A. Jaffe, "Nonpositivity of the energy density in quantized field theories," Nuovo Cim. **36**, 1016 (1965).

[32] M. S. Morris and K. Thorne, "Wormholes in spacetime and their use for interstellar travel: A tool for teaching general relativity," Am. J. Phys. **56**, 395 (1988); M. S. Morris, K. Thorne, and U. Yurtsever, "Wormholes, Time Machines, and the Weak Energy," Phys. Rev. Lett. **61**, 1446 (1988).

[33] S. V. Krasnikov, "Hyperfast Interstellar Travel in General Relativity," Phys. Rev. D **57**, 4760 (1998); K. D. Olum, "Superluminal travel requires negative energies," Phys. Rev. Lett. **81**, 3567 (1998).

[34] A. E. Everett, "Warp drive and causality," Phys. Rev. D **53**, 7365 (1996).

[35] L. H. Ford, "Quantum coherence effects and the second law of thermodynamics," Proc. Roy. Soc. Lond. A **364**, 227 (1978).

[36] L. H. Ford and T. A. Roman, "Restrictions on Negative Energy Density in Flat Spacetime," Phys. Rev. D **55**, 2082 (1997).

[37] L. H. Ford and T. A. Roman, "Averaged energy conditions and quantum inequalities", Phys. Rev. D **51**, 4277 (1995).

[38] C. J. Fewster and S. P. Eveson, "Bounds on negative energy densities in flat space-time," Phys. Rev. D **58**, 084010 (1998).

[39] R. Haag, *Local Quantum Physics*, (Springer-Verlag, Berlin, 1996).

[40] E. E. Flanagan, "Quantum Inequalities in two dimensional Minkowski spacetime," Phys. Rev. D **56**, 4922 (1997).

[41] A. M. Mathai, R. K. Saxena and H. J. Haubold, *The H-Function: Theory and Applications* (Springer, New York, 2010).

[42] J. H. P. Colpa, "Diagonalization of the quadratic boson hamiltonian", Physica **93A**, 327 (1978).

[43] S. Dawson, "Bounds on Negative Energy Densities in Quantum Field Theories in Flat and Curved Space-times", PhD thesis, University of York, UK, 2006.

[44] N. Bogoliubov, "On the theory of superfluidity", J. Phys. **11**, 23 (1947).

[45] See for example A. Quarteroni, F. Saleri, and P. Gervasio, *Scientific Computing with MATLAB and Octave* (Springer, Berlin, 2014), Chap. 5.

[46] C. J. Fewster and M. J. Pfenning, "Quantum energy inequalities and local covariance. I. Globally hyperbolic spacetimes," J. Math. Phys. **47**, 082303 (2006).

[47] A. H. Guth, M. P. Hertzberg and C. Prescod-Weinstein, "Do Dark Matter Axions Form a Condensate with Long-Range Correlation?," Phys. Rev. D **92**, no. 10, 103513 (2015).

[48] E. D. Schiappacasse and M. P. Hertzberg, "Analysis of Dark Matter Axion Clumps with Spherical Symmetry," JCAP **01**, 037 (2018).

[49] M. P. Hertzberg and E. D. Schiappacasse, "Scalar Dark Matter Clumps with Angular Momentum," arXiv:1804.07255 [hep-ph] (2018). Submitted to JCAP.

[50] M. P. Hertzberg and E. D. Schiappacasse, "Dark Matter Axion Clump Resonance of Photons," arXiv:1805.00430 [hep-ph] (2018). Submitted to JCAP.